Quaternary Science Reviews 292 (2022) 107596

Contents lists available at ScienceDirect

Quaternary Science Reviews

journal homepage: www.elsevier.com/locate/quascirev

Volcanism and the Greenland ice cores: A new tephrochronological framework for the last glacial-interglacial transition (LGIT) based on cryptotephra deposits in three ice cores

Eliza Cook [a, b, *], Peter M. Abbott [a, 1], Nick J.G. Pearce [c, 2], Seyedhamidreza Mojtabavi [d, 3], Anders Svensson [b], Anna J. Bourne [a, 4], Sune O. Rasmussen [b], Inger K. Seierstad [b, 5], Bo M. Vinther [b], Joseph Harrison [e], Elliott Street [e], Jørgen Peder Steffensen [b], Frank Wilhelms [d], Siwan M. Davies [a]

[a] Department of Geography, Swansea University, Singleton Park, Swansea, SA2 8PP, UK
[b] Physics of Ice, Climate and Earth, Niels Bohr Institute, University of Copenhagen, 2100, Denmark
[c] Department of Geography and Earth Sciences, Aberystwyth University, Aberystwyth, SY23 3DB, UK
[d] Alfred Wegener Institute, Helmholtz Centre for Polar and Marine Research, Bremerhaven, Germany
[e] Centre for Quaternary Research, Royal Holloway, University of London, Egham, Surrey, TW20 0EX, UK

ARTICLE INFO

Article history:
Received 8 March 2022
Received in revised form
23 May 2022
Accepted 31 May 2022
Available online xxx

Handling Editor: Giovanni Zanchetta

Keywords:
Cryptotephra
Isochron
Greenland
Ice cores
Chronology
Quaternary
Volcanism

ABSTRACT

Chemical profiles from Greenland ice cores show that the frequency of volcanism was higher during the last glacial-interglacial transition (LGIT) and early Holocene, (17–9 ka b2k) than in any other period during the last 110 kyr. This increased frequency has partly been linked to climate-driven melting of the Icelandic ice sheet during the last deglaciation, with regional isostatic changes thought to alter mantle viscosity and lead to more eruptions. Our study is the first to construct a comprehensive tephrochronological framework from Greenland ice cores over the LGIT to aid in the reconstruction of volcanic activity over this period. The framework is based on extensive high-resolution sampling of three Greenland ice cores between 17.4 and 11.6 ka b2k and comprises a total of 64 cryptotephra deposits from the NGRIP, GRIP and NEEM ice cores. We show that many of these tephras are preserved within the core without an associated chemical signature in the ice, which implies that reconstructions of volcanism based solely on glacio-chemical indicators might underestimate the number of events. Single glass shards from each deposit were geochemically characterised to trace the volcanic source and many of these deposits could be correlated between cores. We show that the 64 deposits represent tephra deposits from 42 separate volcanic events, and of these, 39 are from Iceland, two from the north Pacific region (Japan and USA) and one has an unknown source. Six deposits can be correlated to terrestrial and/or marine tephra deposits in the Northern Hemisphere and the remaining 36 are unreported in other archives. We did not locate tephra from the compositionally distinctive Laacher See eruption (~13 ka b2k) in our records. Combining our new discoveries with the previously published tephra framework, raises the number of individual tephra horizons found in Greenland ice over this interval to 50. This significantly improves the regional tephrochronological framework, our knowledge of the eruptive history of Iceland during the LGIT and provides new tephra constraints over key LGIT climate events. Consequentially, this framework can guide sampling strategies of future tephra studies in the terrestrial and marine realms aiming to link these records to the Greenland ice cores to assess regional climate synchroneity.

* Corresponding author. Physics of Ice, Climate and Earth, Niels Bohr Institute, University of Copenhagen, 2100, Denmark.
E-mail address: elizacook@nbi.ku.dk (E. Cook).
[1] Present address: Climate and Environmental Physics, Physics Institute, and Oeschger Centre for Climate Change Research, University of Bern, 3012 Bern, Switzerland.
[2] Present address: Dipartimento di Scienze Biologiche, Geologiche e Ambientali, Università di Bologna, 40126 Bologna, Italy.
[3] Present address: Institute of Geography, University of Bremen, Bremen, Germany.
[4] Present address: School of Geography, Queen Mary University of London, Mile End Road, London E1 4NS, UK.
[5] Present address: The Natural History Museum, Gothersgade 130, København K, Denmark.

https://doi.org/10.1016/j.quascirev.2022.107596

1. Introduction: exploiting ice repositories to establish tephrochronological frameworks

Tephra (derived from the Greek word τέφρα meaning 'ashes') is the pyroclastic fragmental material produced during volcanic eruptions, including ash, pumice and lapilli (Thórarinsson, 1944; 1981; Fisher, 1961). The ash component (<2 mm diameter) of tephra consists of various phases including juvenile glass grains, that can be transported over large distances and deposited instantaneously within days or weeks (Sarna-Wojcicki et al., 1981). Deposition of glass shards over ice sheets and their burial by subsequent snowfall gives rise to a unique and unrivalled repository of volcanic history (e.g. Kurbatov et al., 2006; Dunbar and Kurbatov, 2011; Davies et al., 2014; Bourne et al., 2015). Even low concentrations of glass shards, invisible to the naked eye and referred to as 'cryptotephras', can form stratigraphically distinct deposits in ice cores and marine and terrestrial sediments (e.g. Lowe and Hunt, 2001; Turney et al., 1997; Mortensen et al., 2005; Davies, 2015; Bourne et al., 2015). In addition, the compositional signature of the glass shards is representative of the bulk geochemistry of magma and thus present a distinct fingerprint for tracing deposits to specific volcanic sources and for correlation purposes. Identifying multiple tephra deposits in high-resolution proxy records, such as ice cores, enables the construction of a 'tephrostratigraphy', that can be used to correlate to distal marine and/or terrestrial palaeoarchives if they contain equivalent layers. If these tephra horizons can be dated the resulting 'tephrochronology' allows age estimates to be transferred to all occurrences of a specific layer (e.g. Lowe, 2011). Due to the frequency of volcanic events, the widespread nature of ash dispersal and high preservation potential, tephrochronology is an extensively applied chronological tool for constraining significant climatic and societal changes (e.g. Blockley et al., 2012; Riede, 2008; Davies et al., 2010; Lane et al., 2013; Abbott et al., 2021). Given the high-resolution and annually-resolved chronologies, ice-core records have had a significant role to play in advancing the application of tephrochronology, and are thus key to the goals of INTIMATE (INTegration of Ice-core, MArine, and Terrestrial records) that strives to synchronise records to decipher the sequence, timing, nature and causes of abrupt environmental events during the LGIT (Björck et al., 1998; Lowe et al., 2008; Blockley et al., 2012).

A major advantage of using the Greenland ice cores to build a framework is that each tephra deposit identified in the ice can be assigned an independent age estimate based on the Greenland Ice Core Chronologies such as GICC05 and more recently GICC21, which are derived from annual layer counting of several ice cores (Rasmussen et al., 2006, 2013, 2014; Andersen et al., 2006; Vinther et al., 2006; Svensson et al., 2006; Seierstad et al., 2014, Sinnl et al., 2022). Furthermore, the framework of ash fall events is underpinned by continuous, high-resolution measurements of climate proxy data that provide evidence of the rapid climate changes that punctuated the last glacial period (e.g. Johnsen et al., 1992; Dansgaard et al., 1993; Rasmussen et al., 2014). Around 130 individual ash fall events have been identified in Greenland ice cores older than 25 ka b2k (before 2000 AD), many of which have been traced in more than one ice core and have considerable potential to effect precise tie points between climate records (Grönvold et al., 1995; Zielinski et al., 1996; Davies et al., 2008, 2010, 2014; Abbott et al., 2012; Bourne et al., 2013, 2015, 2016). In contrast, very few tephras have been identified in ice younger than 25 ka b2k, despite the high volcanic frequency reconstructed from the ice-core chemostratigraphic datasets (e.g. Zielinski et al., 1996).

Sulfate concentrations (SO_4^{2-}) (Zielinski et al., 1996; Bigler et al., 2007), electrical conductivity measurements (ECM) of acidity (H^+) and dielectric profiling (DEP) measure impurities in the ice (e.g. Hammer, 1980; Moore et al., 1992; Wolff et al., 1995; Wilhelms et al., 1998; Mojtabavi et al., 2020), and are indicators used to reconstruct past volcanism. For instance, sulfur dioxide (SO_2) released during an eruption can be oxidised into sulfuric acid aerosol (H_2SO_4) in the stratosphere and deposited on the ice surface (Gautier et al., 2019). Such signals can originate from both equatorial and high-latitude eruptions, but their precise volcanic source can only be determined by geochemically analysing any associated volcanic glass shards (Pearce et al., 2004a; Abbott and Davies, 2012). Zielinski et al. (1996) identified SO_4^{2-} signals in the GISP2 ice core and observed the period between 15 and 8 ka b2k to have the longest, most continuous period of enhanced volcanism over the past 110 kyr. A more recent study of sulfur and sulfate records from multiple Greenland ice cores by Lin et al. (2022), adds further support to a volcanically active Northern Hemisphere over the LGIT. Irrespective of the driving mechanisms, the high frequency of volcanic activity observed in the LGIT is not reflected in the existing record of tephra deposits. This is largely a result of limited and discontinuous sampling strategies in early studies, that found 15 deposits, guided predominantly by the presence of visible tephra deposits, the largest acidity peaks in the ECM profile and key tephras (Grönvold et al., 1995; Zielinski et al., 1996; Mortensen et al., 2005). In this study, we build on the work of Bourne et al. (2016) and Cook et al. (2018a) and adopt a detailed tephra sampling strategy to investigate the LGIT in a systematic way.

Volcanism was prevalent in different regions of the Northern Hemisphere during the LGIT (Fig. 1) and thus far of the 15 deposits identified in Greenland ice cores, 13 originate from Icelandic volcanoes, one from Japan and one from an unknown source (Grönvold et al., 1995; Mortensen et al., 2005; Bourne et al., 2016; Cook et al., 2018a) (Fig. 2). One of the key LGIT tephras identified in the GRIP and NGRIP records is the Vedde Ash, a widely distributed Greenland Stadial-1 (GS-1) deposit from Katla with an age of 12,172 ± 114 a b2k (Grönvold et al., 1995; Mortensen et al., 2005). Ash from this eruption has been extracted from numerous terrestrial sites throughout Europe, Scandinavia and Russia and from North Atlantic marine records (e.g. Mangerud et al., 1984; Thornalley et al., 2010; Lane et al., 2012) and has been used to constrain time transgressive environmental changes between Europe and Scandinavia during GS-1 (Lane et al., 2013). Other important marker deposits identified in Greenland ice during the LGIT include two Borrobol-type tephras from Iceland (Cook et al., 2018a), found in Greenland Interstadial-1e (GI-1e) and Towada-Hachinohe (To-H) during GS-2.1a (Bourne et al., 2016), an explosive eruption which occurred in northern Honshu, Japan (Aoki and Arai, 2000) (Fig. 2).

Other studies have demonstrated that ash from Kamchatka, North America, Alaska and the Aleutian Islands (Fig. 1) has also been dispersed to the Arctic during the Holocene and last glacial (Fig. 2, Jensen et al., 2014; Sun et al., 2014; Bourne et al., 2016; van der Bilt et al., 2017; Cook et al., 2018b). The INTIMATE Framework for the Northern Hemisphere also includes well-known LGIT tephras from the Eifel and Mediterranean regions (see Fig. 2 for details and references), but as yet, ash from events such as the Laacher See Tephra, the Neapolitan Yellow Tuff from Campi Flegrei and the Y-1 layer (Etna) have not been found in Greenland.

Here we present a new tephrochronological framework for the LGIT covering 11.6–17.4 ka b2k, based on a semi-continuous sampling approach of three of the deep Greenland ice-core records. The aim was to construct a detailed Greenland tephra event stratigraphy to improve age estimates of known eruptions and identify

Fig. 1. Locations of the NGRIP, GRIP and NEEM ice cores and key volcanic provinces in relation to Greenland and the North Hemisphere. 1: Iceland 2: Jan Mayen 3: The Eifel Region (Germany) 4: The Massif Central (France) 5: The Mediterranean - including the Hellenic Volcanic Arc (Greece), the Campanian Volcanic Arc (Italy), Turkey and Western Asia 6: The Cascades, (Western USA) and Canada (British Columbia and Yukon) 7: Alaska and the Aleutian Arc 8: Kamchatka and the Kurile Islands 9: Japan; 10: North Korea (Changbaishan) and Arxan-Chaihe volcanic field (North East China) 11: The Azores and Canary Islands. Marked on the map are also selected terrestrial and marine sites that contain tephra layers that were correlated to Greenland ice-core tephras presented in this study. MSH: Mount St Helens, Tow: Towada (red border on yellow triangle), SV: Shingo Village (Aoki and Machida, 2006), LA: Loch Ashik (Pyne-O'Donnell et al., 2008), 15–14P: RAPiD-15–14P marine core site (Thornalley et al., 2010), FR: Finglas River (Timms et al., 2019), CP: Crocker Pond, TI: Thin-Ice Pond, VL: Veinot Lake (Pyne-O'Donnell et al., 2016), MD99-2271: marine core site (Guðmundsdóttir et al., 2011). (For interpretation of the references to colour in this figure legend, the reader is referred to the Web version of this article.)

new deposits to add to the INTIMATE framework. Over 240 m of ice was investigated spanning GS-1, GI-1 and GS-2.1a which represents the most comprehensive assessment of tephra preserved during this interval (Fig. 3). Sixty-four new tephra deposits are identified across the 3 cores which represent 42 individual volcanic events. This new framework significantly improves the volcanic history of this period and will guide future tephra studies in other archives. The depths and magma composition of 12 ice-ice tie points from this study were reported in Rasmussen et al. (2013) and Seierstad et al. (2014) to aid GICC05 timescale transfer from NGRIP to GRIP and NEEM and the full details are presented and interpreted here.

2. Methodology

Using a multi-core semi-continuous sampling approach, we explored the NEEM, NGRIP and GRIP ice cores, using three different sampling strategies as described below.

2.1. Ice core sampling and processing strategies: NEEM

2.1.1. Low-resolution screening of NEEM

Continuous, low-resolution (1.1 m) screening of NEEM was performed using discrete meltwater samples, from a meltwater stream normally discarded following measurements via the continuous flow analysis (CFA) system. This was an experimental approach with the aim of maximising cryptotephra identification in ice cores. The CFA system measures numerous parameters from ice-core meltwater synchronously, including soluble and insoluble impurities and the chemical composition of gases trapped in air bubbles (Kaufmann et al., 2008). The CFA system sequentially

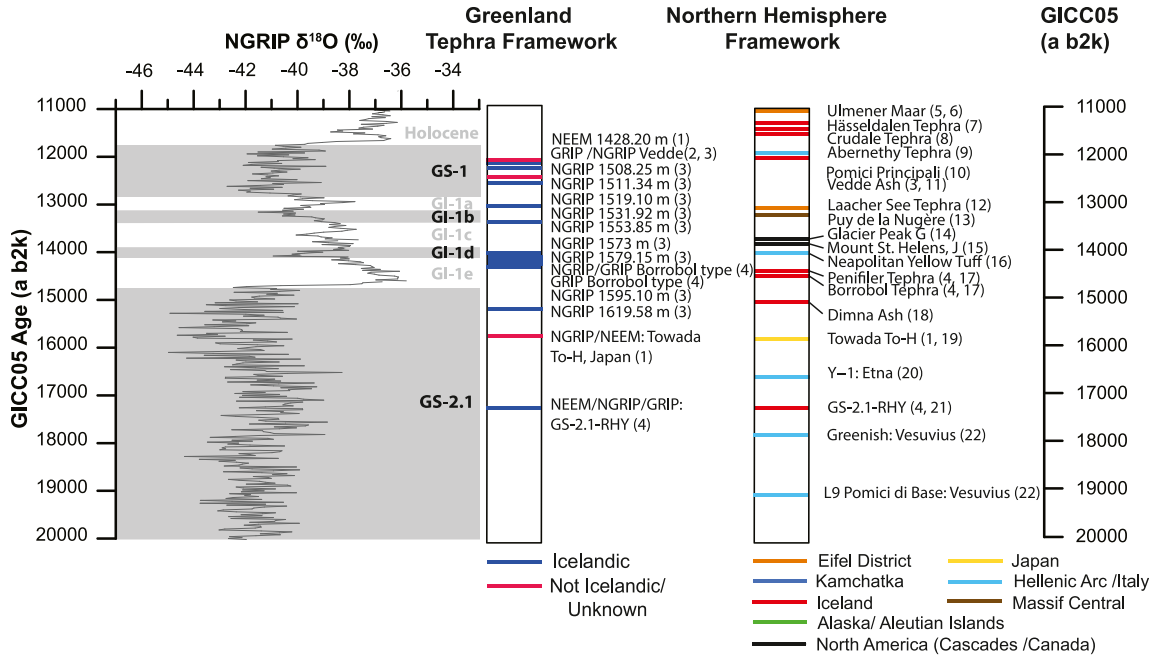

Fig. 2. An overview of the previous Northern Hemisphere tephra framework based on layers identified in Greenland ice and some well-known tephra deposits from key volcanoes (adapted from Blockley et al., 2012). The latter formed the initial search focus of this research. Tephra layer references are as follows: (1) Bourne et al., 2016; (2) Grönvold et al., (1995); (3) Mortensen et al., (2005); (4) Cook et al., (2018a); (5) Zolitschka et al., (1995); (6) Davies et al., (2002); (7) Wastegård et al., (2018) (8) Timms et al., (2019); (9) Matthews et al., (2011); (10) Smith et al., (2011); (11) Mangerud et al., 1984; (12) Riede, 2008; (13) Juvigné et al., 1996; (14) Kuehn et al., 2009; (15) Clynne et al., (2008); (16) Deino et al., (2004) (17) Bronk Ramsey et al., (2015) (18) Koren et al., (2008); (19) Aoki and Arai, (2000); (20) Calanchi et al., (1996); (21) Guðmundsdóttir et al., 2011; (22) Narcisi (1996). The diagram appears alongside Greenland climate events (Rasmussen et al., 2014) for context.

measures 1.1 m long sticks of ice with a 3.1 × 3.1 cm cross section. The ice is melted on a heated plate with a 'clean' inner sample used for high quality continuous measurements, while meltwater from the outer part of each stick is retained for less sensitive discrete analyses, including tephra. A sample of approximately 90 ml per 1.1 m section was collected in individual bottles for tephra analysis. The meltwater samples spanning GS-2 to the early Holocene (106 m long section of ice) were investigated with basic microscopy and used to pinpoint sections of NEEM for subsequent higher-resolution sampling (Fig. 3).

2.1.2. High-resolution 'targeted' sampling of NEEM

High-resolution sampling of NEEM ice was undertaken to explore whether the results of the low-resolution CFA screening could be replicated and if the stratigraphic position of tephra horizons could be refined. This strategy resulted in the sampling of 47.3 m of NEEM ice between 1418 and 1526 m (Fig. 3), based on three criteria: (1) depth intervals with positive tephra occurrences (typically >5 tephra glass shards) in the NEEM CFA samples, comprising 42 CFA sticks (1.1 m long); (2) ice depths spanning published age ranges for important tephras such as the Vedde Ash, Laacher See Tephra, Penifiler Tephra and Borrobol Tephra; and (3) prominent peaks in the ECM record, with 7 events sampled.

2.2. Ice core sampling strategies: NGRIP and GRIP

High-resolution sampling of the NGRIP and GRIP cores (Fig. 3) was based on a broad, semi-continuous sampling approach to maximise the identification of cryptotephras, instead of targeting specific events in the chemical records. In total, 100.10 m of ice was sampled from NGRIP and 60.5 m from GRIP over the LGIT. In an attempt to locate the Laacher See, Borrobol and Penifiler Tephras, the entire GI-1 interval in NGRIP was sampled as well as all ice from GRIP not utilised in prior studies. In GS-2.1a, continuous ice samples from NGRIP and GRIP were taken widely around tephra layers that were already identified in NEEM CFA samples (see section 2.1.1).

2.3. Sample processing and identification techniques

The NEEM, NGRIP and GRIP cores are archived in 55 cm sections at the University of Copenhagen and direct ice samples were taken by sawing off a thin strip of ice (~2 cm^2) from the outer edge of each section of interest. These strips were then divided into three pieces (0–20, 20–40 and 40–55 cm) and the individual samples were melted, producing a typical volume of 35–45 ml. This meltwater was then progressively transferred into test tubes for each individual sample and repeatedly centrifuged for 5 min at 2500 rpm to retain all particulate matter, including tephra, at the bottom of the tube. Supernatant water was discarded, leaving 2–3 ml of water per sample that was evaporated onto frosted glass microscope slides and covered in epoxy resin for optical assessment by high magnification light microscopy. Subsequently, slides containing tephra glass shards were prepared for geochemical analysis. There was a consistent background of 1–3 'tephra resembling' particles per sample, so typically samples containing around 10 grains, or morphologically 'typical' tephra grains in low concentrations were selected. There remains ~90 samples from the three ice cores that contain low concentration (5–10), tiny or ambiguous grains that could benefit further investigation.

2.4. Geochemical analysis and interpretation

Electron probe microanalysis (EPMA) using wavelength dispersive spectrometry (WDS) was used to determine the major (Si, Al, Fe, Mg, Ca, Na, K) and minor (Ti, Mn, P) element composition of individual tephra grains. All major/minor element concentrations (wt%) described here refer to anhydrous concentrations (i.e.

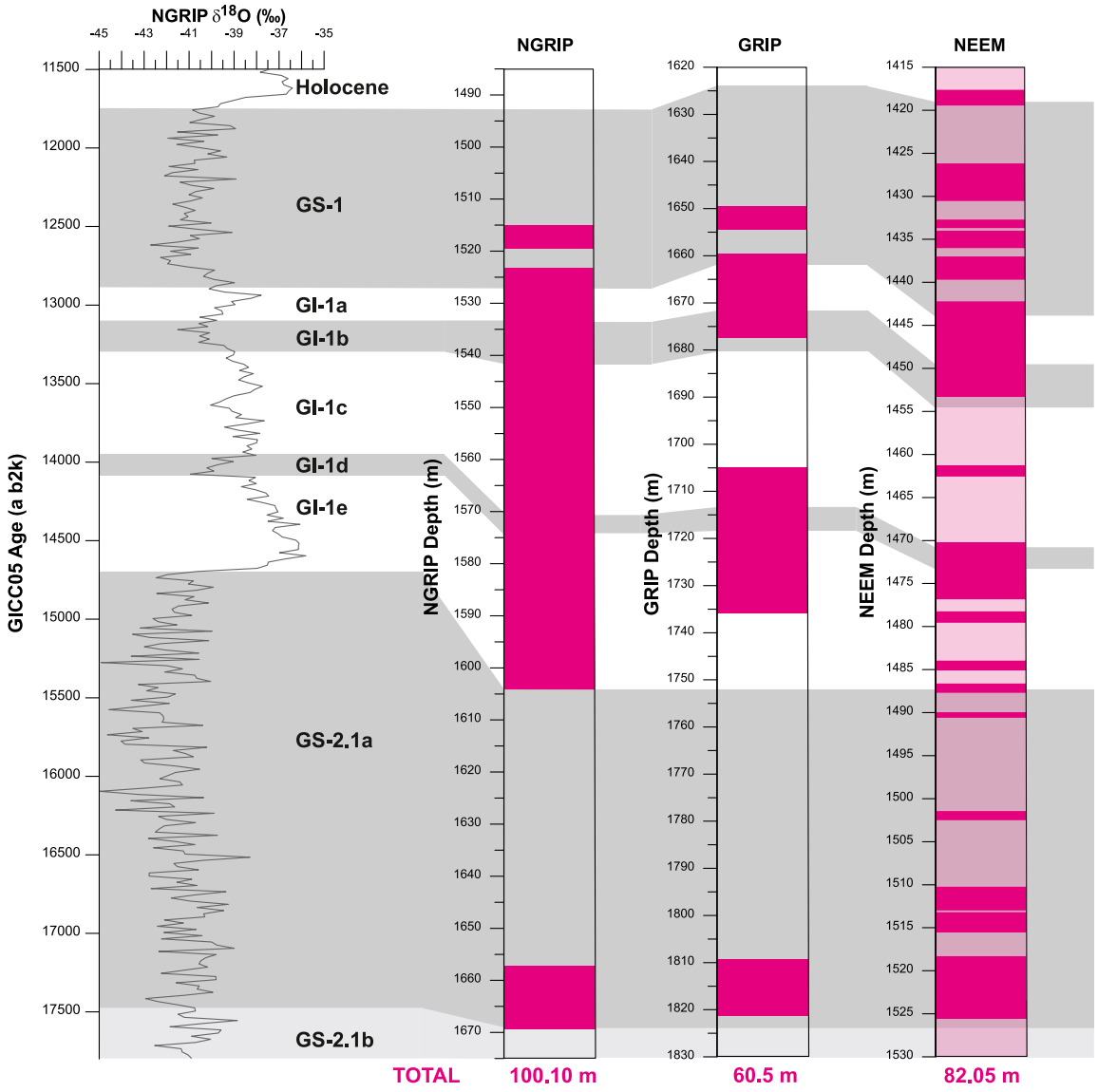

Fig. 3. Sampling strategies for each ice core plotted against climate events from Rasmussen et al. (2014). Individual pink bars denote the depth intervals sampled and the total length of ice retrieved (m) for each core is given at the bottom of the diagram. For NEEM, the transparent, solid pink bar indicates continuous, low resolution (1.1 m) samples (from CFA meltwater retained for discrete analyses) that were screened for tephra, that helped to inform the subsequent high resolution sampling of NEEM (deep pink bars). (For interpretation of the references to colour in this figure legend, the reader is referred to the Web version of this article.)

analytical totals normalised to 100%). EPMA requires flat, exposed horizontal sections through individual grains for efficient electron bombardment and X-ray generation (Hunt and Hill, 1993; Hayward, 2012). These thin sections were produced by grinding down the epoxy mount on tephra-containing slides using silicon carbide paper and the exposed surfaces were then polished using 6, 3 and 1 μm diamond suspension and 0.3 μm alumina powder. All EPMA data were obtained using a Cameca SX100 electron probe micro-analyser at the Tephra Analysis Unit, University of Edinburgh. This system has five wavelength dispersive spectrometers and was calibrated daily using internal standards as described by Hayward (2012). BCR2g and Lipari were analysed daily as secondary standards and monitored to identify any instrumental drift. All sample and secondary standard analyses are provided in Appendix A.

Trace element data were collected from the same glass shards that had undergone EPMA, using laser ablation inductively-coupled plasma mass spectrometry (LA-ICP-MS) at the Department of Geography and Earth Sciences, Aberystwyth University. A Coherent GeoLas ArF 193 nm Excimer LA system with a fluence of 10 Jcm^{-2} at a repetition rate of 5 Hz was used. Analyses were performed using a 10 μm laser beam diameter and spectra were collected over 24 s acquisition periods using a Thermo Finnegan Element 2 sector field ICP-MS. The minor ^{29}Si isotope was used as the internal standard (using normalised SiO_2 results from EPMA) with the NIST 612 reference glass used for calibration, taking concentrations from Pearce et al. (1997). A fractionation factor was applied to the data to account for analytical bias related to the different matrices of the reference standard and the sample material. Data were filtered to remove any analyses incorporating phenocryst phases. Full details of the methods and the LA-ICP-MS operating conditions are given in Pearce et al. (2011) and Pearce et al. (2014), and all trace element concentrations for individual shards are provided in Appendix A.

To determine the provenance of tephra deposits, the oxide concentrations from this study were compared to Icelandic whole rock and tephra glass datasets (see Appendix A) that capture the geochemical range and variability in end member products from

individual volcanoes.

We established ice-ice and ice-terrestrial/marine correlations using three criteria. Firstly, geochemical signatures were matched visually using biplots, to identify compositional overlap between the characterisations of deposits. Secondly, the stratigraphic position of potential matches was used to determine broad chronological validity since some volcanoes, particularly Icelandic centres, can produce tephra horizons with very similar chemical compositions up to thousands of years apart. Thirdly, statistical distance (D^2) (Perkins et al., 1995, 1998; Pearce et al., 2004a, 2008; Denton and Pearce, 2008) and similarity coefficient (SC) (Borchardt et al., 1972) tests were used to statistically compare characterisations. D^2 determines if the sample pairs are statistically different and can be used to dismiss matches whereas SC values > 0.95 strongly indicate that two signatures are from the same volcanic source and could be possible correlatives (Tables 2 and 3). Trace elements can only be compared using statistical difference. For SC comparisons element values >1 wt % is a criterion (typically SiO_2, Al_2O_3, FeO, CaO, NaO_2, K_2O) (Perkins et al., 1998), and for D^2 it is >0.1 wt %. 15 high abundance trace elements (Rb, Sr, Y, Zr, Nb, Ba, La, Ce, Nd, Sm, Eu, Yb, Hf, Th, U) (Pearce et al., 2008) were used in the D^2 comparisons. Critical D^2 values (99% confidence interval) for samples which are statistically different are 18.48 (7 degrees of freedom) and 29.14 (14 degrees of freedom) respectively, with calculated D^2 values for sample comparisons greater than these values showing that samples are statistically different. There are limitations to both methods, which are outlined in Lowe et al. (2017).

2.5. Tephra and chemostratigraphy

Identification of DEP, ECM and sulfate (SO_4^{2-}) peaks associated with cryptotephra deposits was conducted visually in comparison to background concentrations, with peaks defined as approximately three times background, to explore the reliability of these methods for tracing volcanism ice cores. DEP data from NEEM (Mojtabavi et al., 2020, 2022), NGRIP2 (Rasmussen et al., 2013) (using the Wilhelms (2000) set up) and GRIP (Wolff et al., 1997) was utilised. ECM data for NGRIP/NEEM is from Rasmussen et al. (2013) and from Clausen et al. (1997) for GRIP. NGRIP2 SO_4^{2-} data is from Bigler (2004) and Lin et al. (2022). NEEM SO_4^{2-} data are only available as an averaged 20-year resolution record that flattens any peaks and was thus unsuitable for use in this study.

2.6. Tephra age estimates

Each NGRIP/GRIP tephra deposit is assigned a Greenland Ice Core Chronology 2005 (GICC05) age with an uncertainty based on the maximum counting error (MCE) which is derived from the number of ambiguous layers, and can be interpreted as 2σ, where cumulative errors increase with depth (Rasmussen et al., 2006; Vinther et al., 2006). The NEEM core has its own timescale named GICC05modelext-NEEM-1 derived from the transfer of the NGRIP GICC05 chronology to the core using a series of coeval match points, including tephra horizons (Rasmussen et al., 2013).

3. Results

An overview of the tephra deposits found in Greenland ice cores between 11.6 and 17.4 ka b2k is presented in Table 1 and Fig. 4. Sixty-four individual cryptotephra deposits (28 in NGRIP, 22 in GRIP and 14 in NEEM) are identified and geochemically characterised which due to correlations between the cores represent 42 individual volcanic events (Table 1, Figs. 5–7). Seven of these deposits are common to all three ice cores and 12 are common to NGRIP and GRIP (Table 2, Fig. 8). The majority, (36) of the tephra deposits are unreported in any other record (besides Greenland ice) and are attributed to Icelandic sources, specifically to 7 different volcanoes (Table 1). Two deposits originate from volcanoes in the north Pacific region and one has an unknown source. Of the 64 deposits, four horizons (resulting from this work) have been described in associated publications (see layers marked in grey colour, Table 1) and include two GI-1e 'Borrobol-type' layers (Cook et al., 2018a), the GS-2.1a To-H deposit (Japan) in NEEM (Bourne et al., 2016), and a GS-2.1a Borrobol-type layer found in all three cores, named GS-2.1-RHY (Cook et al., 2018a). The full tephra dataset is presented in Appendix A and more detailed layer descriptions are provided in appendix A.

The highest number of volcanic events is found in GI-1, reflecting our comprehensive sampling effort over this period (Fig. 3), plus the longer duration of this climate interval compared to GS-1. In total, 27 individual volcanic events (comprising 38 tephra deposits from the three cores) were found in GI-1, compared to 6 volcanic events (10 deposits) in GS-1 and 9 volcanic events (15 deposits) in GS-2.1a (Table 1, Fig. 4). The concentration of glass tephra shards in the deposits varies widely from just 6 to >5000 shards, however, those with the highest concentrations seem to relate to deposits that can be traced in more than one core (Table 1). The most glass-shard rich event relates to an Öræfajökull deposit in GS-2.1a, originating from the eastern flank zone (EFZ) of Iceland, with over 5000 shards identified, some as large as 60 μm (Table 1). Average grain sizes for deposits are 25–40 μm in diameter with NEEM generally preserving the smallest grains, which is consistent with the findings of the Bourne et al. (2015) study of the 25–45 ka b2k interval in Greenland ice.

Tephra geochemical signatures are dominated by basaltic deposits (mostly transitional alkali and tholeiitic basalts), but rhyolitic deposits are also common during GI-1 and GS-2.1a (Table 1; Figs. 4–7). Deposits originate from about 7 Icelandic centres, with basaltic products originating from Hekla-Vatnafjöll or Vestmannaeyjar, Katla, Grímsvötn, Veiðivötn-Bárðarbunga or Reykjanes (see Appendix B for map). For the silicic tephras, Öræfajökull, Katla, Borrobol-type and Hekla-Vatnafjöll layers are the main sources and compositions we identified. The major element compositions of many deposits overlap in their geochemical ranges (i.e. resembling both Hekla-Vatnafjöll and Vestmannaeyjar or Öræfajökull and Katla or Veiðivötn-Bárðarbunga and Reykjanes), and cannot be distinguished.

In the following sections, we highlight four key aspects of this new framework: i) 19 deposits are identified in more than one core, providing important chronological constraints for validation of the ice-core timescale; ii) six deposits are correlated to previously reported tephras that are preserved in marine and/or terrestrial records including two non-Icelandic deposits originating from Towada, Japan and Mt. St. Helens, USA; iii) 30% of the tephra deposits identified are not associated with a chemo-stratigraphical signal in the ice; and iv) we identify 23 deposits that are likely to be most valuable as correlative tie-points for constraining the rapid climatic events of the LGIT.

3.1. Ice-ice core correlations

The 19 ice-ice correlations presented here build on the data-sets used to validate the timescale transfer of GICC05 from NGRIP to NEEM and GRIP reported in Rasmussen et al. (2013) and Seierstad et al. (2014), respectively. GI-1c was only sampled intensively in NGRIP (Fig. 3), which accounts for the absence of tie-points in this interval. Not all of the correlations are supported by trace element data (Figs. 9–11, Table 2) as LA-ICP-MS could only be performed on deposits with large enough grains. These analyses are relatively noisy due to the low abundance of elements and the low signal to

Table 1
Summary information of all tephra deposits found in NGRIP, GRIP and NEEM ice cores between the early Holocene and GS-2.1a (this study). Deposits are organised by climate event, defined by Rasmussen et al. (2014). Any deposit that can be correlated to another ice core to form a layer is highlighted in **bold**. Summary information includes the ice-core depth intervals (within which each deposit was found), GICC05 ages denoted by $^{\Phi}$ (using the lower ice depth age) for NGRIP/GRIP and GICC05modelext-NEEM-1 ages for NEEM denoted by . A maximum counting error (MCE) is provided for all dates, equivalent to 2σ error as described by Andersen et al. (2006), Vinther et al. (2006) and Rasmussen et al. (2006). Geochemical composition, shard concentrations, average grain size are provided alongside the number of EPMA and LA-ICP-MS analyses obtained from each deposit. LA-ICP-MS analyses are shown in (brackets). The rock type classification is based on Le Maitre et al. (2002). All EPMA analyses were performed at the Tephra Analytical Unit, University of Edinburgh (TAU) and all LA-ICP-MS analyses were performed at Aberystwyth University. Abbreviations for volcanic origins of deposits, refer to the following centres or compositions: Borr-T = Borrobol-type, Gríms = Grímsvötn, H–V = Hekla-Vatnafjöll, Kat = Katla, MSH = Mount St. Helens, Öraef = Öræfajökull, Reyk = Reykjanes, V–B = Veiðivötn-Bárðarbunga,V'mann = Vestmannaeyjar. The presence of ECM, DEP and SO_4^{2-} peaks associated with tephra deposits is indicated with an 'E','D' or 'S'. The DEP data for each core was derived from the following sources: NGRIP2: Rasmussen et al., (2013), GRIP: Clausen et al., (1997); Wolff et al., (1997); Wolff et al., 2005 and NEEM: Mojtabavi et al. (2020), (2022). The ECM data was derived from the following sources: NGRIP2 and NEEM: Rasmussen et al., (2013), GRIP: Clausen et al., (1997). SO_4^{2-} data for NGRIP was from Lin et al. (2022), originally published by Bigler (2004). Layers in *grey italic font* show published ice core layers originating from this study, with the following references **(1)** Bourne et al. (2016); **(4)** Cook et al. (2018a). Additionally, layers with *underlined grey italic font* are ice-core tie points from other studies: **2)**, Grönvold et al. (1995); **(3)** Mortensen et al. (2005).

	NGRIP						GRIP						NEEM								
	Depth (m)	Age$^{\Phi}$ (a b2k) and MCE	Grains/ sample	Grain size (Av. μm)	EPMA/ LA-ICP-MS analyses	ECM/ DEP/ SO4	Depth (m)	Age$^{\Phi}$ (a b2k) and MCE	Grains/ sample	Grain size (Av. μm)	EPMA/ LA-ICP-MS analyses	ECM/ DEP	Depth (m)	Age^ (a b2k) and MCE	Grains/ sample	Grain size (Av. μm)	EPMA/ LA-ICP-MS analyses	ECM/ DEP	Geochem.	Possible Origin	Ref
H													1418.30 - 1418.45	11689 (98)	70	28.2	11	E	TAB	H-V'mann	
													1428.00 - 1428.20	*12127 (114)*	*15*	*25.4*	*5 (4)*	-	*Rhyolite*	*Hekla-Vatn*	*1*
GS-1	*1506.11 - 1506.18*	*12172 (114)*	-	-	*12*	*E/D/S*	*1639.54 - 1639.55*	*12172 (114)*	-	-	*3*	*E/D*	**1429.08 - 1429.13**	***12172 (114)***	**72 (B) 81 (R)**	**27.7**	**7 (4)**	**E/D**	**TAB**	**Katla Vedde Ash**	**2,3**
	1516.75 - 1516.90	**12561 (127)**	**2000**	**34.9**	**10 (10)**	**S**	**1651.50 - 1651.65**	**12561 (127)**	**>5000**	**46.5**	**14 (10)**	**-**	**1437.35 - 1437.55**	**12568 (126)**	**2025**	**34**	**12**	**-**	**Alk/TAB**	**Katla**	
	1518.55 - 1518.75	**12634 (129)**	**105**	**30.9**	**4**	**S**	**1653.50 - 1653.70**	**12634 (129)**	**95**	**32.2**	**10**	**D**							**Thol-bas**	**Grímsvötn**	
	1518.95 - 1519.10	**12646 (129)**	**646**	**32.0**	**13**	**E/D/S**	**1653.85 - 1654.05**	**12646 (129)**	**80**	**31.9**	**9**	**-**							**TAB**	**H-V'mann**	
GI1a													1445.40 - 1445.60	12942 (140)	9	20	2	-	Rhyolite	Borrobol-T	
	1531.60 - 1531.75	**13027 (141)**	**411**	**35.3**	**15 (13)**	**D**	**1668.15 - 1668.35**	**13027 (141)**	**26**	**31.9**	**5 (5)**	**-**							**Thol-Bas**	**Grimsvötn**	
							1669.25 - 1669.45	13047 (141)	8	37.0	2	D							Rhyolite	Borrobol-T	
1b	**1537.25 - 1537.45**	**13186 (145)**	**613**	**36.8**	**15 (8)**	**E/D**	**1674.95 - 1675.15**	**13186 (145)**	**1062**	**36.7**	**16 (7)**	**E**							**TAB**	**Hekla-Vatn**	
	1538.55 - 1538.75	**13222 (146)**	**36**	**41**	**4 (3)**	**E**	**1676.40 - 1676.60**	**13222 (146)**	**70**	**29.5**	**5**	**E/D**							**Rhyolite**	**Öraef/Katla**	
	1540.20 - 1540.40	13270 (147)	6	25	1	D/S													Rhyolite	Hekla-Vatn	
1c1	1541.65 - 1541.85	13304 (148)	7	28	1	E/D													Dacite	Hekla-Vatn	
	1545.70 - 1545.90	13398 (150)	16	32.2	7	-													Thol-Bas	Gríms/V-B	
	1549.35 - 1549.55	13478 (152)	160	30.5	11	E/D													Alk/TAB	H-V'mann	
1c3	1557.45 - 1557.60	13672 (158)	53	30.6	9	-													Rhyolite	MSH	
	1559.25 - 1559.45	13713 (159)	52	23.8	9	E/S													Alkalic Bas	H-V'mann	
	1564.20 - 1564.40	**13822 (162)**	**1500**	**37.2**	**12**	**E/S**	**1706.30 - 1706.50**	**13822 (162)**	**191**	**36.5**	**14**	**E/D**							**Thol-Bas**	**V-B/Reyk**	
1d	*1572.85 - 1573.00*	*14021 (167)*	*2361*	*39.1*	*11 (11)*	*E/D/S*	**1716.35 - 1716.40**	**14021 (167)**	**3122**	**41.6**	**14 (12)**	**E/D**	**1472.20 - 1472.35**	***14027 (168)***	**37**	**41.5**	**10 (9)**	**D**	**TAB**	**Katla**	**3**
GI-1e	**1576.15 - 1576.30**	**14109 (169)**	**45**	**33.6**	**8 (8)**	**E/D**	**1719.85 - 1720.05**	**14109 (169)**	**80**	**37.6**	**3 (3)**	**E**	**1473.85 - 1474.00**	**14113 (170)**	**74**	**37.7**	**3**	**E**	**Rhyolite**	**Öraef/Katla**	
							1723.70 - 1723.90	14183 (171)	51	41.1	10	-							Thol-Bas	Grímsvötn	
	1579.60 - 1579.80	**14191 (171)**	**448**	**41.5**	**10**	**D**	**1724.25 - 1724.45**	**14191 (171)**	**>5000**	**44.0**	**12**	**E**							**Thol-Bas**	**V-B/Gríms**	
	1581.65 - 1581.80	14232 (173)	40	38.9	3	D													Thol-Bas	Grímsvötn	
	1582.55 - 1582.75	*14252 (173)*	*84*	*30.5*	*6 (6)*	*E/D/S*	*1727.55 - 1727.75*	*14252 (173)*	*102*	*33.1*	*7 (5)*	*E/D*							*Rhyolite*	*Borrobol-T*	*4*
	1583.45 - 1583.65	**14270 (174)**	**43**	**25**	**2**	**E/D/S**	**1728.65 - 1728.85**	**14270 (174)**	**100**	**29.5**	**3**	**E/D**							**Rhyolite**	**Hekla-Vat?**	
	1585.30 - 1585.50	14306 (175)	7	32.1	4	-													Thol-Bas	Grímsvötn	
							1733.80 - 1734.00	*14358 (177)*	*90*	*34.3*	*8 (6)*	-							*Rhyolite*	*Borrobol-T*	*4*
	1588.95 - 1589.15	14378 (175)	46	30.2	7	-													Thol-Bas	Unknown	
	1594.10 - 1594.30	14481 (180)	84	34	6	-													Alk/TAB	H-V'mann	
							1739.50 - 1739.65	14455 (179)	83	35.9	9	-							Alk/TAB	H-V'mann	
	1597.05 - 1597.20	**14539 (181)**	**65**	**34.2**	**8**	**-**	**1744.60 - 1744.80**	**14539 (181)**	**21**	**34.5**	**8**	**-**							**Alk/TAB**	**H-V'mann**	
	1597.80 - 1597.95	14553 (181)	14	28.5	4	-													Thol-Bas	Reyk/V-B	
	1604.20 – 1604.35	14684 (185)	500	36.6	17	-													Thol-Bas	Gríms/V-B	
GS-2.1	*1628.18 - 1628.25*	*15684 (226)*	-	-	*10*	*E/S*							*1502.45 - 1502.60*	*15706 (226)*	*22*	*37.4*	*6 (6)*	-	Rhyolite	Towada	1
													1502.45 - 1502.60	15706 (226)	4	28	3	-	Thol-Bas	V-B/Reyk	
													1511.25 - 1511.40	16385 (264)	14	26.6	5	-	Alk/TAB	H-V'mann	
													1519.50 - 1519.65	17004 (300)	59	37.4	10 (10)	-	Alk/TAB	Katla	
	1662.30 - 1662.50	**17187 (311)**	**180**	**30.2**	**5**	**S**	**1814.45 - 1814.65**	**17187 (311)**	**58**	**30**	**6**	**-**	**1522.60 - 1522.80**	**17229 (312)**	**358**	**38.1**	**15 (10)**	**E/D**	**Rhyolite**	**Öraefsjökull**	
	1663.60 - 1663.75	**17238 (313)**	**93**	**27.8**	**10**	**-**	**1816.10 - 1816.30**	**17238 (313)**	**18**	**38.9**	**5 (4)**	**-**	**1523.35 - 1523.50**	**17288 (317)**	**26**	**39.7**	**8 (4)**	**-**	**Thol-Bas**	**V-B/Reyk**	
							1816.50 - 1816.65	17265 (315)	160	40	10 (6)	D							Thol-Bas	V-B/Reyk	
	1663.75 - 1664.30	**17265 (315)**	**>4000**	**61**	**47 (43)**	**S/D**	**1816.50 - 1816.65**	**17265 (315)**	**205**	**60.7**	**10 (7)**	**D**							**Rhyolite**	**Öraefsjökull**	
	1665.40 - 1665.60	*17326 (319)*	*2000*	*47.4*	*15 (13)*	*S*	*1818.15 - 1818.30*	*17326 (319)*	*431*	*49.4*	*12 (7)*	-	*1524.60 - 1524.80*	*17385 (323)*	*125*	*36.8*	*8 (7)*	-	*Rhyolite*	*Borrobol-T GS-2.1-RHY*	*4*

background ratios, owing to the small (10 μm) ablation craters used (see Pearce et al., 2004b, 2011). A summary of the correlations is provided below according to the time-interval in which they are identified.

3.1.1. GS-1

Four tie-points are identified in GS-1; two basaltic Katla layers, including the widespread Vedde Ash, and single layers from Grímsvötn and Hekla-Vatnafjöll (Tables 1 and 2, Figs. 8 and 9). A NEEM deposit at 1429.13 m correlates to the Vedde Ash, dated 12,172 ± 114 a b2k (Rasmussen et al., 2013) which extends its distribution northwards having previously been identified in GRIP and NGRIP (Grönvold et al., 1995; Mortensen et al., 2005). As well as basaltic grains, clear/colourless silicic-type grains were also observed in this deposit, which is typical for the Vedde Ash, which also has intermediate and silicic populations (e.g. Lane et al., 2012). No successful EPMA analyses could be obtained from the small clear grains however. For this horizon the basaltic major element geochemistry is very similar between the NEEM and NGRIP sample pair (Fig. 9a–b), reflected in the SC and D^2 values of 0.967 and 4.52 (Table 2), indicating the dataset pairs are not statistically different. A second basaltic Katla tie-point connects all three cores and is 389 years older, dated 12,561 ± 127 a b2k (Table 1, Fig. 8). In addition to strong major element similarities (Fig. 9c–d), the SC is high, D^2 values are below the critical value (Table 2) and single grain trace element analyses for the samples exhibit similar abundances and element-element ratio trends (Fig. 9e–f, Table 2). Chondrite normalised REE profiles for GRIP and NGRIP slope gently from light rare earth elements (LREE) to the heavy rare earth elements (HREE) and do not exhibit a strong Eu anomaly. The two remaining GS-1 tie-points form a stratigraphically close couplet between NGRIP and GRIP (Fig. 8, Table 2) and comprise a tholeiitic layer from Grímsvötn dated 12,634 ± 129 a b2k (Fig. 9g–h) and a Hekla-Vatnafjöll layer dated 12,646 ± 129 a b2k (Fig. 9i–j), originating from the southern flank zone (SFZ) in Iceland.

3.1.2. GI-1a-e

The 10 tie-points in GI-1 are mostly NGRIP-GRIP correlations, although two tephra tie-points are found in all three cores (Table 2, Fig. 8). From these isochrons, we highlight three key deposits.

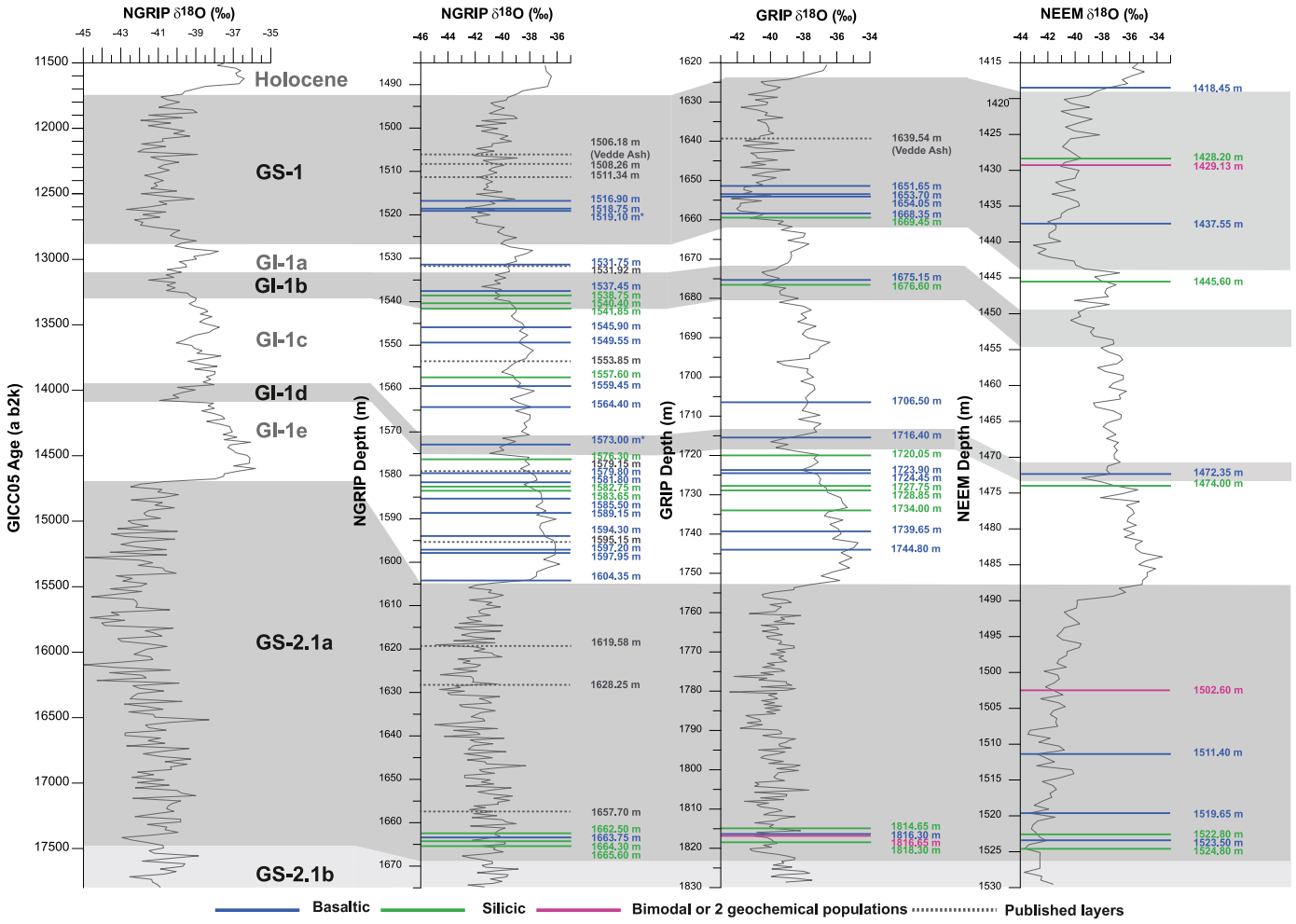

Fig. 4. The new LGIT Greenland ice-core tephrochronology, presenting 64 cryptotephra layers resulting from this study against depth between 11.6 and 17.4 ka b2k. Individual deposits are represented by bars; blue (basaltic), green (silicic), pink (bimodal/or two different geochemical populations from separate eruptions), and are plotted against $\delta^{18}O$ measured from each core (GRIP (20-year resolution): Johnsen et al., 2001; NGRIP: NGRIP members, 2004 (20-year resolution); NEEM (55 cm mean): Gkinis et al., 2021). The diagram also shows previously published tephra deposits (NGRIP: Mortensen et al., 2005 and GRIP: Grönvold et al., 1995) with grey dashed lines, and layers with a * denotes published NGRIP deposits (Mortensen et al. 2005) that were resampled to obtain additional grains for EPMA. Onset/termination of climate periods between the Holocene and GS-2.1 have been defined by Rasmussen et al. (2014). (For interpretation of the references to colour in this figure legend, the reader is referred to the Web version of this article.)

Firstly, the transitional alkali basalt Hekla-Vatnafjöll horizon in GI-1b, that links NGRIP and GRIP at 13,186 ± 145 a b2k (and coincides with a negative excursion in the ice core $\delta^{18}O$ records (Fig. 10c-e, g-h)). Secondly, a basaltic isochron in GI-1d from Katla links NGRIP, GRIP and NEEM at 14,021 ± 167 a b2k (Fig. 10c–d, f-h, Section 3.2.3.). Trace element analyses of the Katla samples reveal very similar REE ratios between NGRIP and GRIP, however, the NEEM sample has a similar profile, but lower REE ratios, and when statistically compared, exceeds the critical D^2 value (Table 2, Fig. 10f). This could be due to sensitivity differences between the analytical periods producing noisier analyses and larger standard deviations for low abundance elements (Pearce et al., 2008). However, NEEM concentrations plot along the same trend lines as NGRIP and GRIP, and biplot ratios demonstrate correspondence between all three cores (Fig. 10g–h).

Thirdly, a GI-1e Öræfajökull or Katla isochron links NGRIP, GRIP and NEEM and is dated to 14,109 ± 169 a b2k (Figs. 8 and 10i-m). This tie-point is tentative due to low viable EPMA analyses obtained for NEEM (3) and GRIP (3) and differences in NEEM SiO_2 and Na_2O concentrations, where secondary standard data from the NEEM analytical session show both elements were not within the recommended values. Nevertheless, trace element profiles and ratios for NGRIP and GRIP provide additional evidence to support this correlation (Fig. 10k-m).

3.1.3. GS-2.1a

There are 5 tie-points in GS-2.1a (Tables 1 and 2, Fig. 8). Geochemical characterisations and statistical tests were important factors for testing correlations, given the few chronostratigraphic match points in this period. The youngest tie-point extends the To-H isochron from Japan (15,706 ± 226 a b2k), from NEEM to NGRIP, where the NGRIP deposit was previously reported by Mortensen et al. (2005) but published as 'unknown origin'. The NEEM occurrence of To-H was reported in Bourne et al. (2016) but here we establish the ice-ice correlation to NGRIP and to additional proximal deposits (Fig. 11a–b, Section 3.2.4). Also in this period is a tie-point attributed to Öræfajökull (Fig. 11c–d), with an age of 17,187 ± 311 a b2k closely followed by a tie-point that originates from either Veiðivötn-Bárðarbunga or Reykjanes dated 17,238 ± 313 a b2k (Fig. 11h–i). Both of these tie-points connect all three ice cores with good statistical and geochemical agreement (Table 2). Next is another Öræfajökull isochron linking NGRIP-GRIP at 17,265 ± 315 a b2k (Fig. 11c–g) with good geochemical similarity, high SC and D^2 values below critical values (Table 2). This older

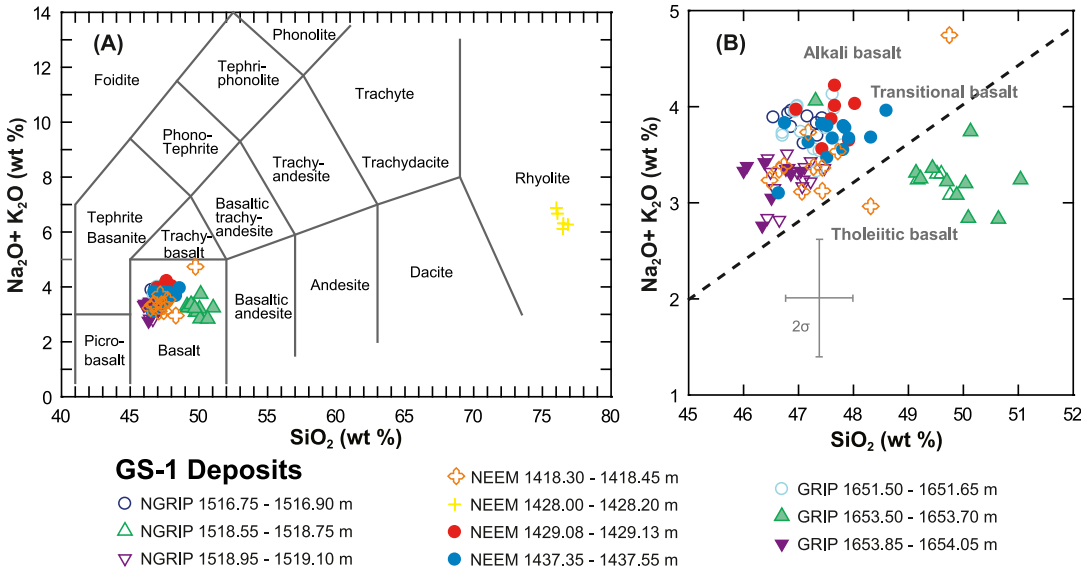

Fig. 5. (A) Glass analyses from Holocene to GS-1 cryptotephra deposits from NGRIP, GRIP and NEEM cores, plotted against magma type – which is assigned on the content of total alkali ($Na_2O + K_2O$) vs silica (SiO_2) (TAS) (Le Maitre et al., 2002). Geochemical data are normalised to 100% (anhydrous basis). Error bars represent 2 standard deviations (2σ) of replicate analyses of the BCR2g and Lipari obsidian secondary standards. (B) Close-up of basaltic compositions, where populations are separated by a dashed alkaline/tholeiitic division line from Irvine and Baragar (1971).

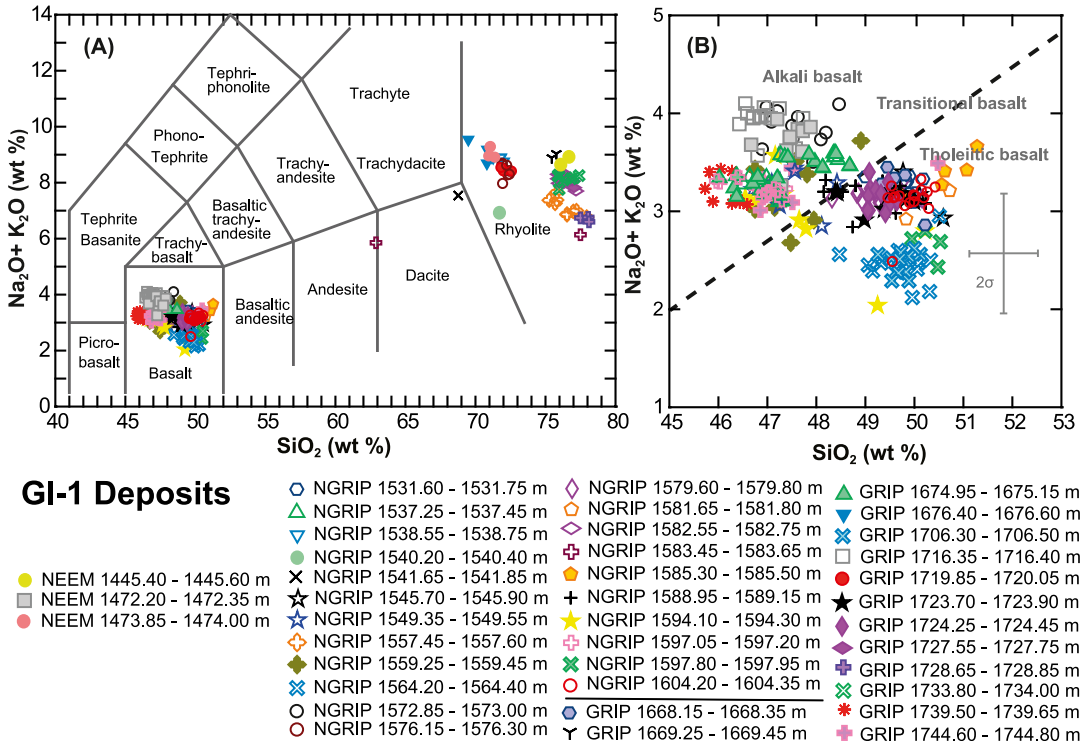

Fig. 6. (A) Glass analyses from GI-1 cryptotephra deposits from NGRIP, GRIP and NEEM cores, plotted against magma type – which is assigned on the content of total alkali ($Na_2O + K_2O$) vs silica (SiO_2) (TAS) (Le Maitre et al., 2002). Geochemical data are normalised to 100% (anhydrous basis). Error bars represent 2 standard deviations (2σ) of replicate analyses of the BCR2g and Lipari obsidian secondary standards. (B) Close-up of basaltic compositions, where populations are separated by a dashed alkaline/tholeiitic division line from Irvine and Baragar (1971).

Öræfajökull layer displays distinguishing features, including a sub-population with lower CaO concentrations and a negative FeO–CaO covariation trend (Fig. 11c–d) that may indicate magma evolution over the course of the eruption. The average trace element profiles for this tie-point are very similar between the full NGRIP dataset (Fig. 11e–g) and the GRIP deposit (D^2: 7.755), with steep gradients between the LREEs and MREEs and negative Eu anomalies. Geochemical data from a series of NGRIP samples over a 55 cm interval show that Öræfajökull likely produced tephra over a ~20-year period and a more complete range of tephra products has been captured in NGRIP, but only partially in GRIP. High resolution re-sampling over the 55 cm NGRIP section (see Appendix B) shows

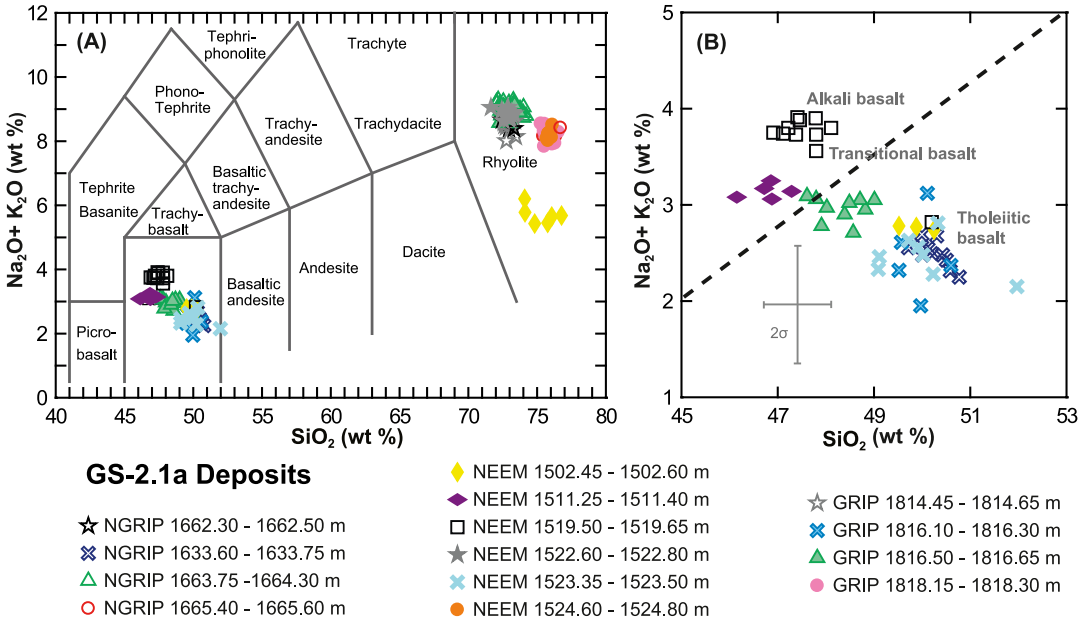

Fig. 7. (A) Glass analyses from GS-2.1a cryptotephra deposits from NGRIP, GRIP and NEEM cores, plotted against rock type – which is assigned on the content of total alkali ($Na_2O + K_2O$) vs silica (SiO_2) (TAS) (Le Maitre et al., 2002). Geochemical data are normalised to 100% (anhydrous basis). Error bars represent 2 standard deviations (2σ) of replicate analyses of the BCR2g and Lipari obsidian secondary standards. (B) Close-up of basaltic compositions, where populations are separated by a dashed alkaline/tholeiitic division line from Irvine and Baragar (1971).

that grains were located between 1663.75 and 1664.30 m, with the younger samples (1663.75–1664.05 m) containing low shard concentrations, before peaking with over 4000 grains in 1664.05–1664.15 m. Counts remained relatively high in 1664.15–1664.30 m with over >350 grains. Conversely, the GRIP deposit was constrained within a 15 cm interval with 205 grains. Trace element profiles for NGRIP shards show the older horizons (i.e. first erupted) to be most evolved and have the greatest overlap with the GRIP composition (Fig. 11g). Less evolved material, potentially from lower in the magma chamber, is found in the NGRIP youngest sample (1663.95–1664.15 m).

The oldest tie-point in this period is GS-2.1-RHY, dated 17,326 ± 319 a b2k and described by Cook et al. (2018a).

These tie-points fill a gap where there are few ECM/DEP match points between GICC05 and GICC05modelext-NEEM-1 due to high glacial dust content that acts to neutralise acidity (Wolff et al., 1995) (Fig. 12). The absence of match points over a wide interval of >150 m means that the time-scale transfer relies on interpolation between ECM points. The precision of the synchronization is typically within 10 cm in intervals with good ECM/DEP match points (Rasmussen et al., 2008), and the four new tephra tie-points reveal a slight NGRIP/NEEM offset from the interpolation, of about 0.5 m in GS-2.1a.

3.2. Ice core correlations to marine and terrestrial deposits

Five isochrons identified in this study allow precise tie-points to be established between Greenland ice-cores and terrestrial and/or marine records (Table 3, Figs. 8 and 13). These include the Vedde Ash, Mount St. Helens-J set, a GI-1d isochron, To-H and the (Borrobol-like) GS-2.1-RHY isochron. Additionally, two GI-1e Borrobol-like deposits may correlate to the well-known but chronologically complex Borrobol-Tephra. Full details of each isochron are provided in Table 3 and Cook et al. (2018a) provides information on the Borrobol-like tephras and GS-2.1-RHY.

3.2.1. GS-1 Vedde Ash, 12,172 ± 114 a b2k

A basaltic NEEM Katla deposit at 1429.13 m can be linked to the Vedde Ash (Table 3), marking the most northerly occurrence of this tephra. Fig. 13a–d shows the geochemical agreement to the terrestrial and marine sites. The Vedde Ash has also been found in GRIP and NGRIP, with large associated spikes in ECM, DEP and SO_4^{2-} (Fig. 14a).

3.2.2. GI-1c3 Mount St. Helens set J, 13,672 ± 158 a b2k

In NGRIP a low-alkali rhyolite deposit in GI-1c3 at 1557.60 m is correlated to a broad tephra unit known as the set J from Mount St. Helens (MSH) (Fig. 8, Table 3), located in the Cascade volcanic arc in western USA (Fig. 1). The layer is not associated with chemo-stratigraphic peaks (Fig. 14b) in the ice. The set J, dated 13.86–12.80 cal ka BP (Clynne et al., 2008), is a series of closely-spaced eruptions referred to as the 'Swift Creek' phase, which produced widespread ash deposits of near identical composition between GI-1 and early GS-1 (Clynne et al., 2008; Mullineaux, 1996). The NGRIP layer geochemically resembles set J type reference material as well as distal set J deposits found in three eastern seaboard lakes; Crocker Pond (Maine, USA), Thin-Ice Pond and Veinot Lake in Nova Scotia, Canada (Pyne-O'Donnell et al., 2016) (Fig. 13e–h). The ice and terrestrial samples share the same linear covariation trend between SiO_2 and Al_2O_3, and SC and D^2 values do not reveal differences between the NGRIP and MSH set J unit datasets (Fig. 13f, Table 3).

3.2.3. GI-1d Katla, 14,021 ± 167 a b2k

The GI-1d basaltic Katla isochron is traced in all three ice cores and correlates to the K3 Tephra found in South Iceland Rise marine core RAPiD-15-4 (Thornalley et al., 2010, 2011) and tentatively to a terrestrial deposit found in a lake core, Isl-W, from Loch Ashik on the Isle of Skye, western Scotland (Pyne-O'Donnell et al., 2008) (Figs. 1, 8 and 13, Table 3). Both studies proposed tie-points between their deposits and the NGRIP deposit at 1573 m, originally discovered by Mortensen et al. (2005). We traced the same layer in NEEM at 1472.35 m and GRIP at 1716.40 m, thus extending the

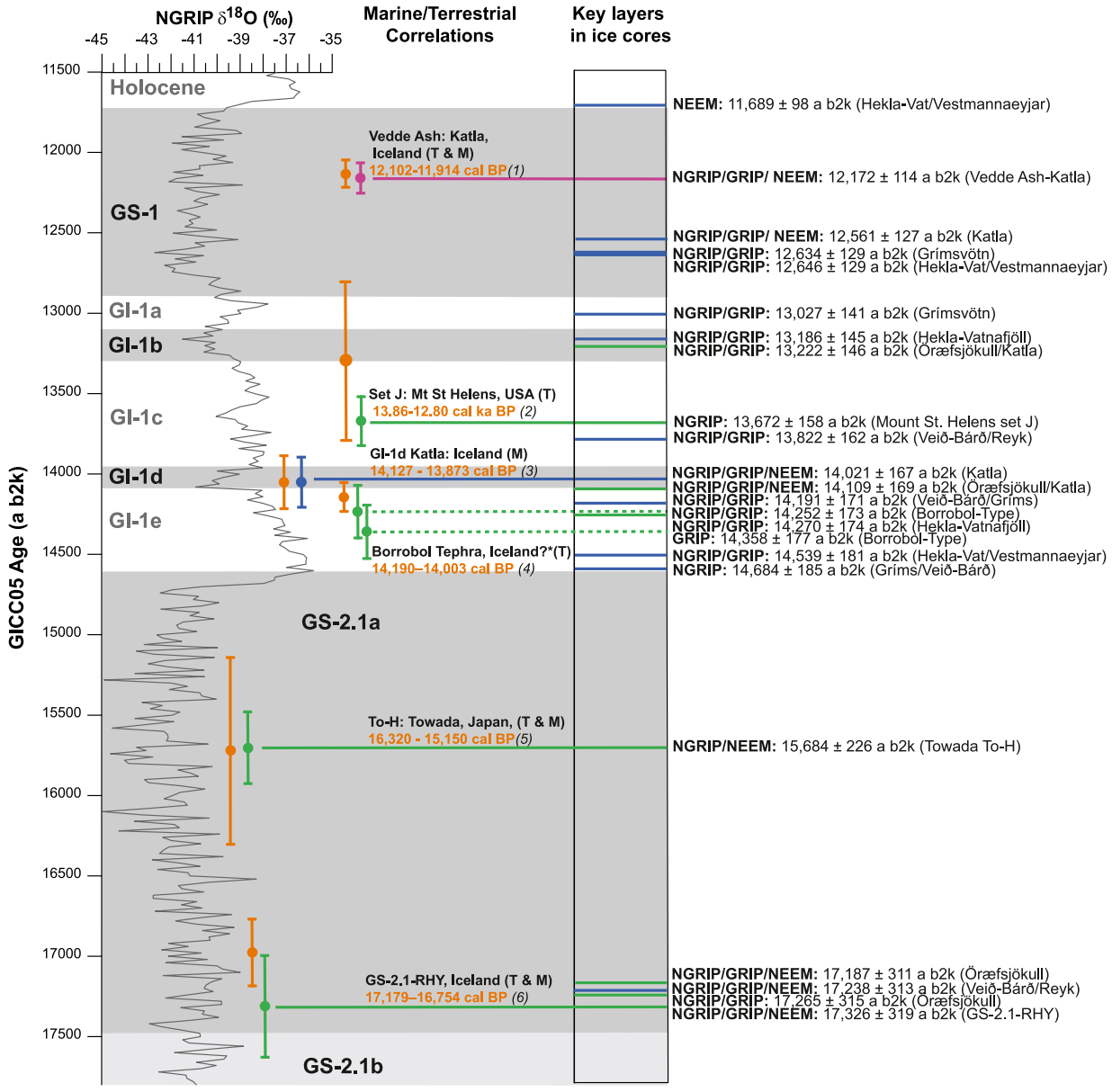

Fig. 8. A summary of tephra tie-points and most useful ice-core deposits (based on stratigraphy and composition) established from our LGIT framework. Tie-points have been established between the ice cores and also with marine (M) and/or terrestrial records (T). Blue bars denote tie-points with Icelandic basalt composition, whilst green bars denote tie-points with a silicic composition. GICC05 ages are provided for all ice core tie-points, with the exception of the Holocene NEEM deposit that has a GICC05modelext-NEEM-1 age. Error bars (2σ) on tephra dates are given for both ice core and terrestrial/marine ages (the latter are shown in orange colour). Terrestrial/marine core tephra ages are from: (1) Vedde Ash: Bronk Ramsey et al. (2015). (2) Mount St. Helens set J Tephra: Clynne et al. (2008). (3) Katla K3 Tephra: Thornalley et al. (2011). (4) Borrobol Tephra: Bronk Ramsey et al. (2015). (5) Towada To-H: Ogawa et al. (2011). (6) GS-2.1-RHY: Cook et al. (2018a). *Two GI-1e Borrobol-type deposits are likely tie-points to the terrestrial Borrobol Tephra (see Cook et al., 2018a). (For interpretation of the references to colour in this figure legend, the reader is referred to the Web version of this article.)

isochron in Greenland, and we also present more NGRIP shard analyses to strengthen the correlation. The event is also associated with ECM, DEP and SO_4^{2-} peaks (Fig. 14c).

In the RAPiD-15–4P marine core in the North Atlantic (Fig. 1), the K3 Tephra forms a 1.5 cm thick visible horizon in a cold oscillation equivalent to GI-1d, as defined by stratigraphic shifts in % abundance of *Neogloboquadrina pachyderma* sinistral (Nps), a planktonic temperature-sensitive foraminifera species (Thornalley et al., 2010). Thornalley et al. (2010, 2011) correlated the K3 layer to NGRIP 1573 m, and used this tie-point in the construction of the RAPiD-15–4P age model, in which the K3 is dated to 13.87–14.13 cal ka BP (Table 3). A slight offset is seen in Al_2O_3 values between the glass shard analyses from the ice versus the marine deposit (Fig. 13i-l), which could be due to the use of different microprobes.

The major element compositions of the three ice-core horizons are also similar to a basaltic Katla deposit in the Loch Ashik core Isl-W between 933 and 934 cm. Bivariate plots show geochemical similarity between the Katla deposits found in the ice cores and the lake record (Fig. 13m-p) and SC and D^2 values support the correlations (Table 3). In Isl-W, the Katla deposit is located at the same depth as the Penifiler Tephra, which is found in numerous records across the British Isles in the Older Dryas cold interval, equivalent to GI-1d (e.g. Matthews et al., 2011; Timms et al., 2019) and dated to 14,063–13,808 cal BP (95%; IntCal13) in the Scottish Abernethy Forest lake core (Bronk Ramsey et al., 2015). We therefore assume

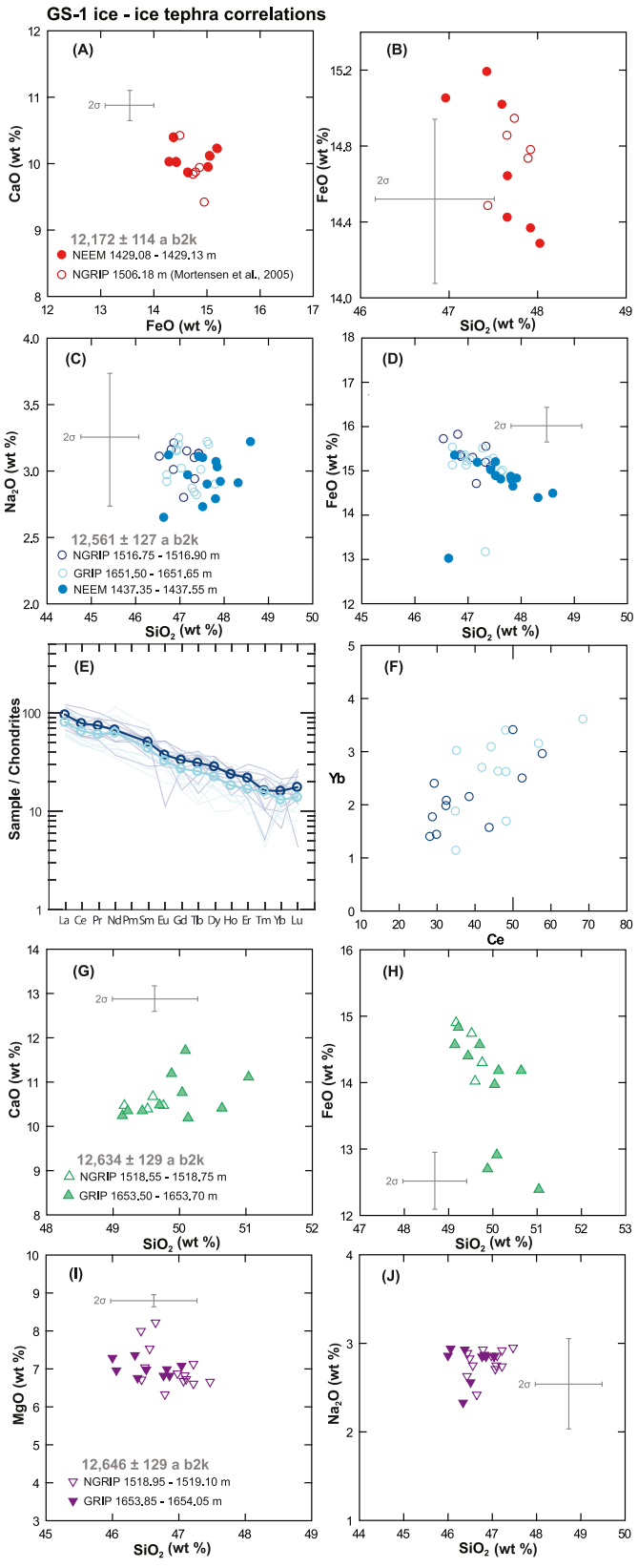

Fig. 9. (A-D, G–J) Major element-element biplots showing the geochemical relationship between corresponding ice-core deposits. Geochemical data are normalised to 100% (anhydrous basis) and analyses with totals below 94 %wt were excluded. Error bars in all diagrams represent two standard deviations (2σ) of replicate analyses of the BCR2g and Lipari obsidian secondary standards, for basalt and rhyolitic analyses respectively. (E) Single grain and average chondrite-normalised REE profiles for NGRIP 1516.90 m and GRIP 1651.65 m, and (F) element-to-element biplots for trace elements based on absolute concentrations (ppm) from single grains. Chondrite compositions are from McDonough and Sun (1995). All ages are from GICC05.

the Abernethy Forest Penifiler Tephra age range, and apply it to the Isl-W Katla basaltic deposit. This age agrees with the GICC05 age and we therefore follow the tentative correlation to NGRIP 1573 m proposed by Pyne-O'Donnell et al. (2008), which also extends the isochron to NEEM and GRIP. Although the correlation makes sense chronologically, a robust chronology needs to be constructed for Isl-W core, to validate this tie-point.

3.2.4. GS-2.1a Towada To-H, 15,706 ± 226 a b2k

Distinct low-alkali rhyolite horizons found in NEEM at 1502.60 m (Bourne et al., 2016) and NGRIP 1628.25 m (Mortensen et al., 2005) correlate to the To-H eruption (Bourne et al., 2016), which produced significant chemostratigraphic peaks in both ice cores (Fig. 14e–f) in Greenland, and also a weak signal in Antarctica (Lin et al., 2022). To-H is a marker-deposit on Honshu Island, Japan (e.g. Hayakawa, 1985; Machida and Arai, 2003) (Fig. 1), having been found in numerous marine cores, close to the Japan Trench, in the western North Pacific Ocean (e.g. Aoki and Arai, 2000; Aoki and Machida, 2006:, 2006; Ikehara et al., 2013).

We compare geochemical data for the Greenland tephra deposits to the ignimbrite and co-ignimbrite phases of the eruption from Shingo Village proximal deposits (Fig. 13q) (Aoki and Machida, 2006) and To-H from marine cores (Aoki and Sakamoto, 2003) (Fig. 13r-t). All bivariate plots exhibit similar trends in FeO–CaO and CaO–MgO and negative linear covariation between SiO_2–TiO_2, and the datasets are not statistically separable (Table 3), supporting the correlation.

3.3. The prevalence of tephra deposits with coeval ice chemical signatures

To assess how the volcanic events from this study are recorded in the ice chemostratigraphy, we conducted a basic visual assessment to estimate the number of tephras that occur in association with peaks in ECM, DEP and SO_4^{2-} records (SO_4^{2-} available for NGRIP only). The tephra deposits we present are located within samples that are typically 15 or 20 cm in resolution. We found that of the 68 cryptotephras presented in Table 1 (including the tie-points published in other studies), 40 (59%) are associated with chemical peaks that occur within the same 15 or 20 cm sample as the tephra samples, although with the exception of Vedde and To-H, many peaks are small compared to baseline values of surrounding ice (e.g. Fig. 14d, g-i). For NEEM, just 35% of tephras are associated with ECM and/or DEP peaks in their sample ranges, while for GRIP the association is 45%. If we focus on NGRIP, which also has a SO_4^{2-} record and the most cryptotephras (31), we find that 70% of these deposits have peaks within the same sample from one or more chemical records. Fifty-eight percent of NGRIP ECM/DEP peaks (which typically occur coevally) and 45% of SO_4^{2-} peaks are associated with tephra samples. Only five NGRIP tephras are associated with perceptible peaks found across all three chemical records.

For GS-2.1a there are few ECM/DEP associations for all cores, likely due to the neutralisation signals by high dust content, around 10x higher in GS-2.1a than in GI-1 (see Ruth et al., 2003). However, given the low interstadial dust content, it is surprising that there are no tephras associated with any of the chemical records in the first half of GI-1e for NGRIP and GRIP (Table 1). Between GI-1d and GS-1 there is a good correspondence between tephras and peaks for NGRIP and GRIP, while there are some occurrences in NEEM, which has fewer tephras overall.

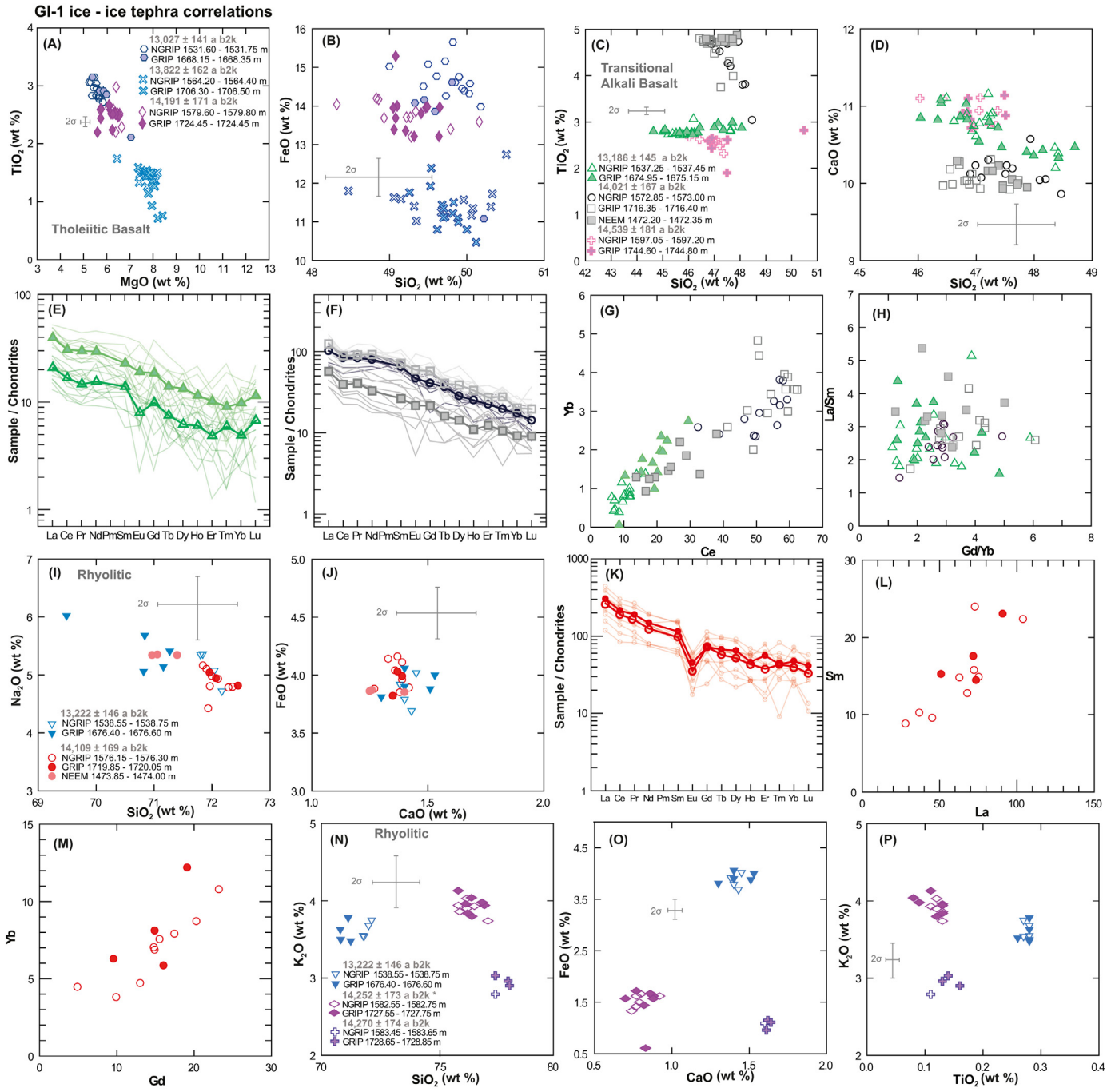

Fig. 10. GI-1a-e ice-ice correlations(A-D, I-J, N–P): Major element-element biplots showing the geochemical relationship between corresponding ice-core deposits. Geochemical data are normalised to 100% and analyses with totals below 94 %wt were excluded. Error bars in all diagrams represent 2σ of replicate analyses of the BCR2g and Lipari obsidian secondary standards, for basalt and rhyolitic analyses respectively. (E-F and K): Single grain and average chondrite-normalised REE profiles for ice-ice correlations, and (G-H, L-M): element-to-element biplots for trace elements based on absolute concentrations (ppm) from single grains or ratios. Chondrite compositions are from McDonough and Sun (1995). All ages are from GICC05. * denotes correlaton previously published by (Cook et al., 2018a).

These are useful estimates of the relationship between Icelandic tephra deposits and their chemical signatures in Greenland ice cores, but further stratigraphic refinement is required to conclude unequivocally that the source of peaks and tephras found in common samples are the same. It is possible that some associated peaks were produced by eruptions in other regions at the same time, or are responding to influences other than volcanism, such as sea-salt aerosols and ammonium, deposited after storms and forest burning events (Fuhrer et al., 1996).

We identify evidence of local differences in acid deposition in Greenland, with some tie-points having associated peaks in just one core. For example, the To-H deposit in NGRIP has an associated ECM signal and huge SO_4^{2-} spike of 3000 ppbw (Fig. 14e), but the same deposit in NEEM does not have a related ECM nor DEP signal (Fig. 14f). This could be due to signal neutralisation in NEEM during stadial conditions, or depositional differences between the sites (e.g. Wolff et al., 2005).

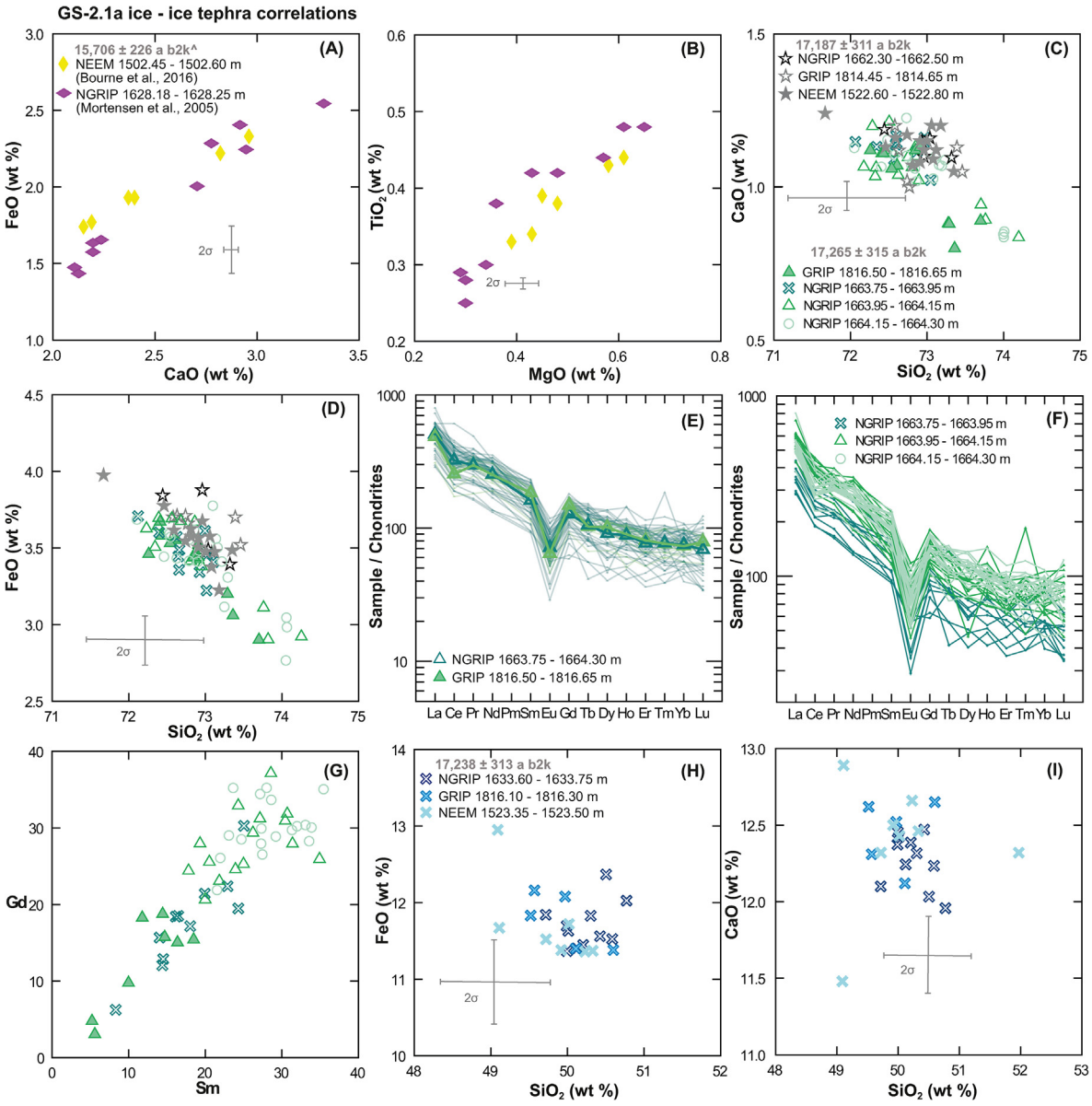

Fig. 11. GS-2.1a ice-ice correlations. (A-D, H–I): Major element-element biplots showing the geochemical relationship between corresponding ice-core deposits. Geochemical data are normalised to 100% and analyses with totals below 94 wt% were excluded. Error bars represent two 2σ of replicate analyses of the BCR2g and Lipari obsidian secondary standards, for basalt and rhyolitic analyses respectively. (E and F): Single grain and average chondrite-normalised REE profiles for ice-ice correlations, and (G): element-to-element biplot for trace elements based on absolute concentrations (ppm) from single grains. Chondrite compositions are from McDonough and Sun (1995). All ages are from GICC05, except one marked with ^, which has a GICC05modelext-NEEM-1 age.

4. Discussion

This work provides some additional details about the Icelandic eruptions that contributed to the sulfate peaks identified by Zielinski et al. (1996) and Lin et al. (2022) during a period of continuously enhanced volcanism during the deglacial. Between 11.67 and 17.39 ka b2k, Lin et al. (2022) identified 175 volcanic events with sulfate deposition rates (corrected for ice layer thinning) larger than 20 kg km^{-2} (above background) in Greenland. To put in context, a volcanic mass deposition rate of 20 kg km^{-2} is half Tambora size (39.7 kg km^{-2}: Sigl et al., 2015), and thus represents quite a large SO_2 injecting event. We find that 9 of events identified by Lin et al. (2022) are likely associated to the eruptions identified in this study (8 Icelandic and To-H) and 4 others are attributed to Icelandic events published in Mortensen et al. (2005). The origins of the remaining 162 events are unaccounted for due to a lack of associated tephras as well as sampling gaps between 15 and 17 ka b2k, but will almost certainly include other Icelandic, Northern Hemisphere (Fig. 1) or equatorial eruptions that did not deposit tephra grains over Greenland. Additionally, we find that over half of the volcanic events presented here do not have an associated SO_4^{2-} signature. These eruptions were most likely smaller-scale (<20 kg km^{-2}) meaning previous estimates of volcanic frequency have been underestimated.

4.1. Key deposits and tephra constraints on environmental change

The LGIT tephrostratigraphic framework for Greenland is dominated by Icelandic volcanic products, with just two non-Icelandic events found in the entire record. Even so, our

Table 2
NEEM, GRIP and NGRIP tephra deposits are correlated to form tie-points between the cores, organised here by climate event. Depth interval, rock type and volcanic provenance is also provided for each set of tie-points. Tie-points that have been used by Seierstad et al. (2014) for timescale transfer of the GICC05 timescale to GRIP are marked with *, and tie-points that have been used by Rasmussen et al. (2013) for the timescale transfer of GICC05 to GICC05modelext-NEEM-1 are marked with ¤. Similarity coefficients (SC) (Borchardt et al., 1972) and statistical difference (D^2) (Perkins et al., 1995, 1998) calculations are given for all for major element sample pairs (data normalised to 100%). For major elements, elements >1 wt% and 0.1 wt% were used to calculate SC, and D^2 respectively, based on the method from Hunt et al. (1995). Values > 0.95 suggest products are from the same volcanic eruption. The value for testing the D^2 values at the 99% confidence interval is 18.48 (7 degrees of freedom). Where associated trace elements pairs were available, D^2 was performed using 14 elements, and the value is given in brackets (T). The value for testing D^2 values at the 99% confidence interval is 29.14 (14 degrees of freedom). All ages are from GICC05, except Towada (marked with ^) (GS-2.1a) which has a GICC05modelext-NEEM-1 age. See Table 1 for abbreviations of volcanic centres.

Event	NGRIP range (m)	GRIP depth (m)	NEEM depth (m)	Age (a b2k and MCE)	Rock Type	Origin	SD and D^2 values
GS-1	1506.11–1506.18 ¤	1639.54–1639.55 ¤	1429.08–1429.13 ¤	12,172 (114)	TAB	Katla (Vedde)	NGRIP/NEEM; SD: **0.967**, D^2: **4.520**
GS-1	1516.75–1516.90 *	1651.50–1651.65*	1437.35–1437.55	12,561 (127)	Alk/TAB	Katla	NGRIP/GRIP; SD: **0.987**, D^2: **0.520** ***(2.660 T)***
							NGRIP/NEEM: SD: **0.983**, D^2: **7.385**
							NEEM/GRIP; SD: **0.981,** D^2: **1.895**
GS-1	1518.55–1518.75 *	1653.50–1653.70 *		12,634 (129)	Thol-bas	Gríms	SD: **0.981**, D^2: **1.434**
GS-1	1518.95–1519.10 *	1653.85–1654.05 *		12,646 (129)	TAB	H-V'mann	SD: **0.981,** D^2: **1.286**
GI-1a	1531.60–1531.75 *	1668.15–1668.35 *		13,027 (141)	Thol-Bas	Gríms	SD: **0.960**, D^2: **4.094** ***(12.848 T)***
GI-1b	1537.25–1537.45 *	1674.95–1675.15 *		13,186 (145)	TAB	Hekla-Vatn	SD: **0.992**, D^2: **0.845 (25.309 T)**
GI-1b	1538.55–1538.75	1676.40–1676.60		13,222 (146)	Rhyolite	Öræf/Katla	SD: **0.967**, D^2: **8.170**
GI-1c	1564.20–1564.40 *	1706.30–1706.50 *		13,822 (162)	Thol-Bas	V–B/Reyk	SD: **0.976**, D^2: **0.921**
GI-1d	1572.85–1573.00 *¤	1716.35–1716.40 *	1472.20–1472.35 ¤	14,021 (167)	TAB	Katla	NGRIP/GRIP; SD: **0.979** D^2: **3.123** ***(30.140 T)***
							NGRIP/NEEM: SD: **0.975**, D^2: **14.954*(87.173 T)***
							NEEM/GRIP; SD: **0.975,** D^2: **9.206** ***(95.671 T)***
GI-1e	1576.15–1576.30	1719.85–1720.05	1473.85-1474.00	14,109 (169)	Rhyolite	Öræf/Katla	NGRIP/GRIP; SD: **0.988**, D^2: **2.727**
							NGRIP/NEEM: SD: **0.957**, D^2: **21.290**
							NEEM/GRIP; SD: **0.955,** D^2: **32.852**
GI-1e	1579.60–1579.80 *	1724.25–1724.45 *		14,191 (171)	Thol-Bas	V–B/Gríms	SD: **0.988**, D^2: **0.886**
GI-1e	1582.55–1582.75 *	1727.55–1727.75*		14,252 (173)	Rhyolite	Borrobol-Type	SD **0.979**:, D^2: **1.088** ***(3.283 T)***
GI-1e	1583.45–1583.65	1728.65–1728.85		14,270 (174)	Rhyolite	Hekla-Vatn?	Too few data points
GI-1e	1597.05–1597.20 *	1744.60–1744.80 *		14,539 (181)	Alk/TAB	H–V'mann	SD: **0.988**, D^2: **0.495**
GS-2.1a	1628.18–1628.25 *		1502.45–1502.60	15,706 (226)^	Rhyolite	Towada Japan	NGRIP/NEEM; SD: **0.940**, D^2: **3.727**
GS-2.1a	1662.30–1662.50 *	1814.45–1814.65 *	1522.60–1522.80	17,187 (311)	Rhyolite	Öræfs	NGRIP/GRIP; SD: **0.985** D^2: **1.808**
							NGRIP/NEEM: SD: **0.982**, D^2: **3.841**
							NEEM/GRIP; SD: **0.969,** D^2: **4.163**
GS-2.1a	1663.60–1663.75	1816.10–1816.30	1523.35–1523.50	17,238 (313)	Thol-Bas	V–B/Reyk	NGRIP/GRIP; SD: **0.987**, D^2: **2.192**
							NGRIP/NEEM: SD: **0.984**, D^2: **1.200**
							NEEM/GRIP; SD: **0.984,** D^2: **1.812**
GS-2.1a	1663.75–1664.30 *	1816.50–1816.65 *		17,265 (315)	Rhyolite	Öræf	NGRIP/GRIP; SD: **0.983**, D^2: **1.337** ***(7.755 T)***
GS-2.1a	1665.40–1665.60 *	1818.15–1818.30 *	1524.60–1524.80	17,326 (319)	Rhyolite	GS-2.1-RHY Borrobol-Type	NGRIP/GRIP; SD: **0.995**, D^2: **0.172 (0.945 T)**
							NGRIP/NEEM: SD: **0.985**, D^2: **1.855**
							NEEM/GRIP; SD: **0.983,** D^2: **1.068**

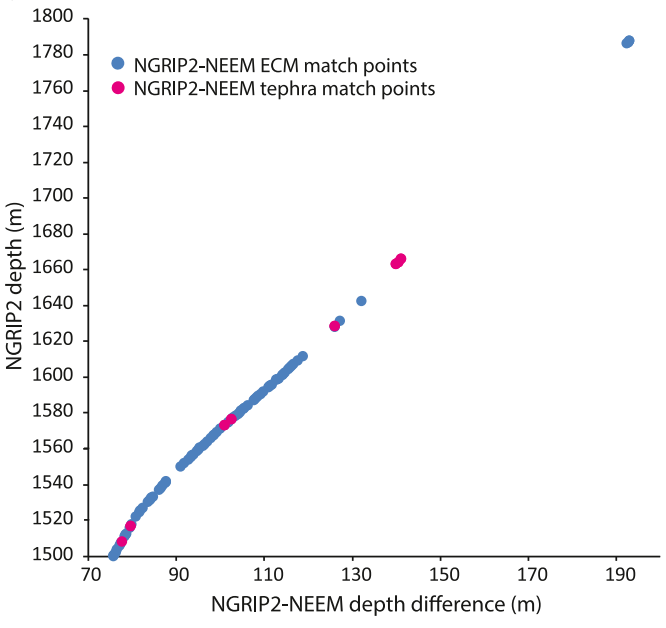

Fig. 12. Eight GS-1 to GS-2.1a tephra match points between NEEM and NGRIP2 are plotted against depth difference (m) between the two cores. Blue circles are ECM match points of Rasmussen et al. (2013), showing the extended gap in match points within GS-2.1. (For interpretation of the references to colour in this figure legend, the reader is referred to the Web version of this article.)

discoveries significantly improve the Northern Hemisphere tephrochronological framework, revealing numerous, previously unreported volcanic events that will help guide future work aiming to trace these deposits in other palaeoclimate records. When combined with 15 tephra deposits identified in prior studies (Fig. 2), the updated Greenland tephra framework contains 50 individual ash deposits between 11.6 and 17.4 ka b2k (Fig. 4). All of these deposits have the potential to be traced in other palaeoarchives to assess synchroneity and regional time transgressive changes in environmental change.

Of these 50 deposits, we highlight 23 key deposits in Fig. 8 that we consider most unique, based on their stratigraphic position and distinctive composition, and includes the 19 deposits identified in more than one ice core and five deposits that are traced in other archives. In particular, three deposits fall close to rapid climatic transitions. At the onset of the Holocene a previously unreported basaltic deposit, resembling Hekla-Vatnafjöll and Vestmannaeyjar in NEEM, is dated to 11,689 ± 98 a b2k, holds huge potential to explore the relative timing of regional environmental changes related to this transition. Deposited just 14 years after the Holocene onset in the ice, its identification in lake or marine records, could help constrain the end of the Pleistocene across Northern Europe, North America and the North Atlantic. A GI-1e rhyolitic deposit with an Öræfajökull or Katla composition connects all three ice cores at 14,109 ± 169 a b2k, around 34 years before the GI-1d transition. Furthermore, another GI-1e NGRIP basaltic deposit

Table 3
NEEM, GRIP and NGRIP tephra deposits with their potential counterparts in the terrestrial and/or marine realms. Geochemical composition, volcanic provenance and tephra name are listed for each set of tie-points. TAB = transitional alkali basalt. Ice-core correlations to terrestrial **(T)** or marine **(M)** sites are distinguished. Samples used for geochemical comparison are given in a separate column, with references. Details of SC and D^2 calculations are provided in Table 2.

Event	Ice core deposit(s)	Deposit previously published in an ice core	Geochem	Origin	Terrestrial/ Marine Correlation	Tephra name	Age of deposit & site(s) compared to	SD and D^2 values
GS-1	NEEM 1429.13 m **12172 ± 114 a b2k**	GRIP 1639.55 Grönvold et al. (1995) NGRIP 1506.18 Mortensen et al. (2005)	TAB	Katla	Terrestrial and Marine	Vedde Ash	**12,102–11,914 cal BP** (Bronk Ramsey et al., 2015) **MD99–2271, North Iceland Shelf:** 697.5–703.5 cm **(M)** Guðmundsdóttir et al. (2011) **Loch Ashik, Scotland:** 584 cm **(T)** Lane et al. (2012)	NEEM/MD99-2271 - SD: **0.975**, D^2: **0.888** NEEM/Loch Ashik - SD: 0.**977**, D^2: **1.643**
GI-Ic3	NGRIP 1557.60 m **13672 ± 158 a b2k**		Rhyolite	Mount St. Helens USA	Terrestrial	MSH-J set	**(13.86-12.80 cal ka BP** (Clynne et al., 2008) **Thin Ice Pond, Nova Scotia**: MSH-JY **(T)** **Veinot Lake, Nova Scotia**: MSH-J **(T)** **Crocker Pond, Maine USA**: MSH-J **(T)** Proximal Reference UA2482: JY **(T)** Pyne-O'Donnell et al. (2016)	NGRIP/Thin Ice Pond - SD: **0.980**, D^2: **3.980** NGRIP/Veinot Lake - SD: **0.955**, D^2: **1.298** NGRIP/Croker Pond - SD: **0.975**, D^2: **2.217** NGRIP/Ref: UA2482 - SD: **0.966**, D^2: **2.171**
GI-1d	NEEM 1472.35 m NGRIP 1573.00 m GRIP 1716.40 m **14021 ± 167 a b2k**	NGRIP 1573 m Mortensen et al. (2005)	TAB	Katla	Terrestrial and Marine	Loch Ashik Katla (T) (tentative) and K3 Tephra (M)	14.127 -13,873 cal BP (Thornalley et al., 2011) **Lock Ashik Isl-W, Scotland:** 933–934 cm **(T)** Pyne-O'Donnell et al. (2008) **15-4P core, North Atlantic:** 500 cm **(M)** Thornalley et al. (2011)	NGRIP/Ashik - SD: **0.975**, D^2: **4.421** NEEM/Ashik- SD: **0.979**, D^2 **4.421** GRIP/Ashik - SD: **0.978**, D^2 **15.378** NGRIP/15–4P - SD: **0.952**, D^2: **4.623** NEEM/15–4P - SD: **0.964**, D^2 **4.724** GRIP/15–4P - SD: **0.961**, D^2 **4.730**
GI-1e	GRIP 1727.75 m NGRIP 1582.75 m **14252 ± 173 a b2k** GRIP 1734.00 m **14358 ± 177a b2k**	GRIP 1727.75 m NGRIP 1582.75 m GRIP 1734.00 m Cook et al. (2018a)	Rhyolite	Borrobol-type, Iceland	Terrestrial	Borrobol Tephra	**14,190–14,003 cal BP** (Bronk Ramsey et al., 2015) **Borrobol, Scotland**: BO521 cm (T) Lind et al. (2016)	NGRIP 1582.75 & GRIP 1727.75/Borrobol BO521 - SD: **0.966**, D^2 **3.036 (*10*.078 TE)** GRIP 1734/BO521 - SD: **0.969**, D^2 **1.812 (5.137 TE)**
GS-2.1a	NEEM 1502.60 m **15706 ± 226 a b2k**	NGRIP 1628.25 m Mortensen et al. (2005) NEEM 1502.60 m Bourne et al. (2016)	Rhyolite	Towada, Japan	Terrestrial and marine	To-H	**16,320–15,150 cal BP** (Ogawa et al., 2011) **Forearc terrace of Japan Trench:** Hole 1150A: 45–56 cm **(M)** Hole 1151C: 110–112 cm **(M)** KH94-3 LM8 (cube 3-28) **(M).** Aoki and Arai. (2000), Aoki and Sakamoto. (2003)	NEEM/1150A - SD: **0.955**, D^2: **3.250** NEEM 1151C - SD: **0.951**, D^2: **4.906** NEEM KH94-3 - SD: **0.938**, D^2: **1.516**
GS-2.1a	NEEM 1524.80 m GRIP 1818.30 m NGRIP 1665.60 m **17326 ± 319 a b2k**	NEEM 1524.80 m GRIP 1818.30 m NGRIP 1665.60 m Cook et al. (2018a)	Rhyolite	Borrobol-type, Iceland	Marine	GS-2.1-RHY Borrobol-type	**17,179–16,754 cal BP** (Jarvis, 2013) **MD99–2271, North Iceland Shelf:** 805.5–807.5 cm **(T)** Guðmundsdóttir et al. (2011) and Cook et al. (2018a)	NGRIP/MD99-2271 - SD: **0.990**, D^2: **0.836** NGRIP/MD99-2271 - SD: **0.990**, D^2: **0.725** NGRIP/MD99-2271 - SD: **0.986**, D^2: **2.022**

from Grímsvötn or Veiðivötn-Bárðarbunga is located just 8 years after the GS-2.1a/GI-1e transition.

Besides the Vedde Ash (hereafter VA), four further valuable GS-1 deposits are yet to be located in the marine or terrestrial realms, including a distinct NEEM rhyolite (12,127 ± 114 a b2k) probably originating from Hekla-Vatnafjöll (Figs. 4 and 5a) that is just 45 years younger than the VA. A layer that connects all three cores is dated 12,561 ± 127 a b2k, 389 years older than the VA, and has a basaltic Katla composition almost identical to the VA (Figs. 8 and 9). Terrestrial or marine studies should only attribute deposits to the VA if they contain rhyolitic grains to avoid miscorrelation, since the basaltic compositions of these deposits are indistinguishable. Other NGRIP-GRIP tie-points from Grímsvötn (12,634 ± 129 a b2k) and Hekla-Vatnafjöll or Vestmannaeyjar (12,646 ± 129 a b2k) (Fig. 8) are not close to climatic transitions, but are nevertheless useful when considered as part of the wider GS-1 tephrostratigraphy.

The numerous deposits found in GI-1 have the potential to constrain the short-lived climate fluctuations within this period. For instance, the short 203-year GI-1a warm period contains three deposits, including a basaltic Grímsvötn layer, that connects NGRIP to GRIP (13,027 ± 141 a b2k). In the 84-year long GI-1b cold event, notable layers include a basaltic Hekla-Vatnafjöll NGRIP-GRIP tie-

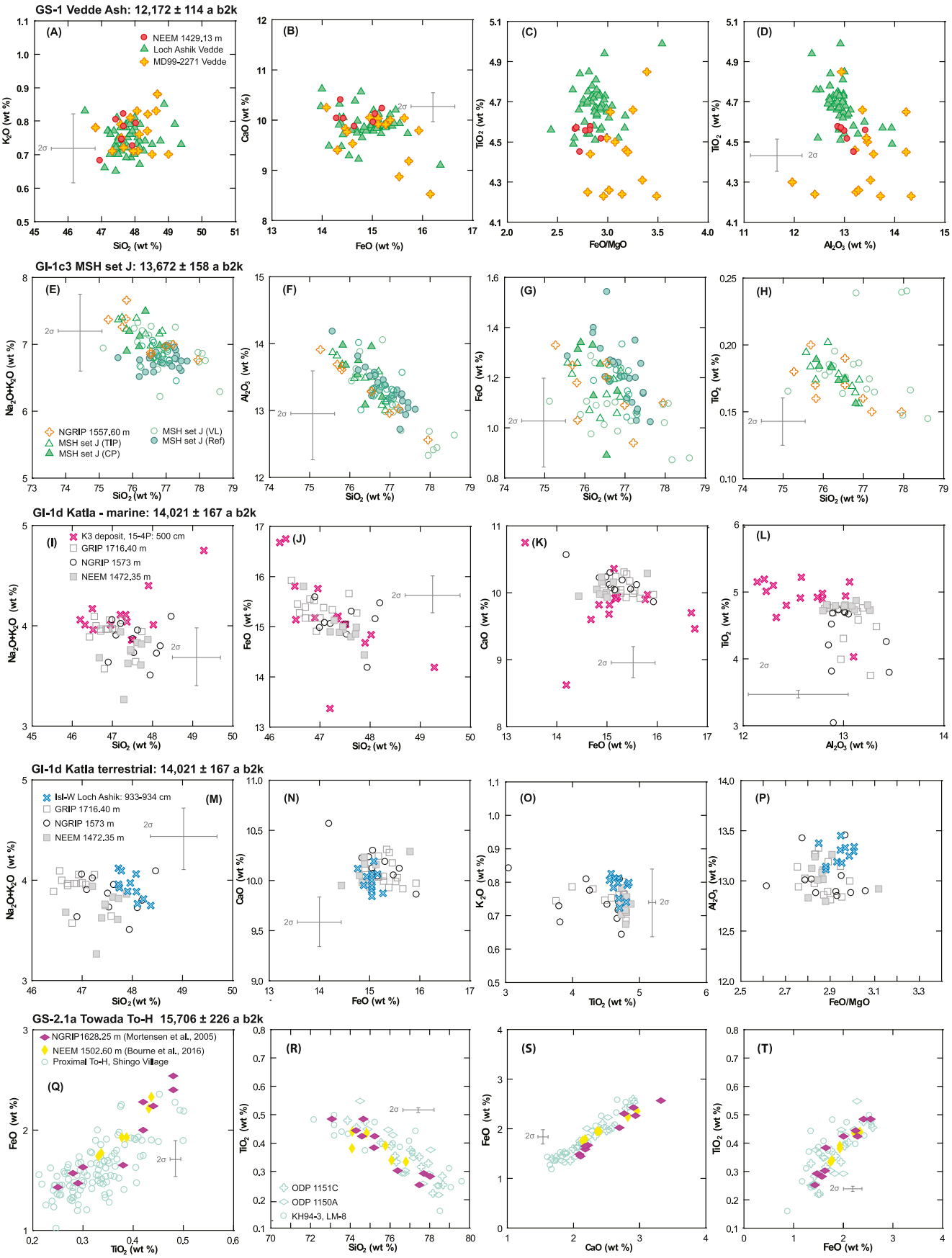
GS-1 Vedde Ash: 12,172 ± 114 a b2k
(A)
NEEM 1429.13 m
Loch Ashik Vedde
MD99-2271 Vedde
K2O (wt %)
SiO2 (wt %)
(B)
CaO (wt %)
FeO (wt %)
(C)
TiO2 (wt %)
FeO/MgO
(D)
TiO2 (wt %)
Al2O3 (wt %)
GI-1c3 MSH set J: 13,672 ± 158 a b2k
(E)
Na2O+K2O (wt %)
NGRIP 1557.60 m
MSH set J (TIP)
MSH set J (CP)
MSH set J (VL)
MSH set J (Ref)
(F)
Al2O3 (wt %)
(G)
FeO (wt %)
(H)
TiO2 (wt %)
GI-1d Katla - marine: 14,021 ± 167 a b2k
(I)
K3 deposit, 15-4P: 500 cm
GRIP 1716.40 m
NGRIP 1573 m
NEEM 1472.35 m
(J)
(K)
(L)
GI-1d Katla terrestrial: 14,021 ± 167 a b2k
(M)
Isl-W Loch Ashik: 933-934 cm
(N)
(O)
(P)
GS-2.1a Towada To-H 15,706 ± 226 a b2k
(Q)
NGRIP1628.25 m (Mortensen et al., 2005)
NEEM 1502.60 m (Bourne et al., 2016)
Proximal To-H, Shingo Village
(R)
ODP 1151C
ODP 1150A
KH94-3, LM-8
(S)
(T)

point (13,186 ± 145 a b2k) and rhyolitic layers with Öræfajökull or Katla (13,222 ± 146 a b2k) and Hekla-Vatnafjöll compositions (13,270 ± 147 a b2k). Six layers have been found in GI-1c, and the most unique is the NGRIP MSH set J deposit (Fig. 13e–h). Our discovery extends a layer from the complex MSH-J set to its most northerly position. Set J deposits have also been traced to three distal sites along the east coast of Canada (>4000 km away from source) (Pyne-O'Donnell et al., 2016) and, via a single grain, to the Finglas River site in Ireland, >7000 km away from source (Timms et al., 2019) (Fig. 1). The full potential for using MSH set J as a tie-point to compare climatic records between different environments has yet to be realised, and requires that the stratigraphic sequence of events comprising the set J are resolved. This is challenging considering indistinguishable geochemistry (B. Jensen, pers. comm, 2021).

A basaltic Katla layer located in the 162 year-long GI-1d cold event connects all three cores just before the GI-1c boundary and has been correlated to marine core RAPiD-15–4P in the North Atlantic Rise, with agreement in proxies, including low $\delta^{18}O$ values in Greenland and increases in %Nps (Thornalley et al., 2011). The same layer is tentatively correlated to the Loch Ashik record from the British Isles (Pyne-O'Donnell et al., 2008). In GI-1e, a newly discovered rhyolitic layer from Öræfajökull or Katla connects NGRIP-GRIP-NEEM just 34 years before the GI-1d onset, and there are two closely-spaced Borrobol-type layers in GI-1e dated 14,252 ± 173 a b2k and 14,358 ± 177 a b2k, the occurrences and implications of which have been discussed in Cook et al. (2018a). These two Borrobol-type deposits probably equate to the well-known Borrobol Tephra, found in terrestrial records of the British Isles (i.e. it is likely the Borrobol Tephra represents amalgamation of tephra from both of the GI-1e events identified in the ice-cores) but a firm correlation is precluded due to the indistinguishable composition and close stratigraphic association (Fig. 8). We recommend these deposits be sought out as key markers in any LGIT studies using tephras to improve their chronologies, but care should be taken if only one layer of Borrobol-type composition is found. GI-1e is otherwise dominated by previously unreported basaltic deposits of tholeiitic composition from Grímsvötn and Veiðivötn-Bárðarbunga and alkali/transitional alkali composition from Hekla-Vatnafjöll or Vestmannaeyjar, which are useful in the stratigraphic context if traced to other records.

Combined with the work of Mortensen et al. (2005), there are now 11 tephra layers within GS-2.1a (Fig. 4). Four closely spaced tie-lines are recorded between 17.18 and 17.32 ka b2k that should be used to aid timescale transfer between ice cores and direct any future terrestrial and marine tephra sampling strategies. The deepest GS-2.1a layer is dated 17,326 ± 319 a b2k, and has the oldest known Borrobol-type composition. This isochron was traced in all three ice cores and to three North Iceland Shelf marine cores (Fig. 8) (Cook et al., 2018a). Just 60 years prior, a series of silicic eruptions from Öræfajökull is recorded over ~22 years (17,243–17,265 ± 315 a b2k) in NGRIP. We interpret the changing trace element compositions with depth as a temporal change in magma composition over the course of a series of eruptions, attributed to a zoned magma chamber (Fig. 11e–f). The events are only partially captured in GRIP and completely missing in NEEM, thus reinforcing the importance of a multi ice-core sampling approach over key periods of interest. A younger Öræfajökull eruption occurs ~45 years earlier, dated 17,187 ± 311 a b2k, and is captured in all three ice cores. If a single Öræfajökull event is located in marine/terrestrial records, we have identified two criteria that may help validate correlations. Firstly, the older deposit has a unique sub-population characterised by higher SiO_2 and lower FeO and CaO values (Fig. 11c–d). Secondly, a layer (dated 17,238 ± 313 a b2k with Veiðivötn-Bárðarbunga or Reykjanes composition (Table 1, Fig. 8) is found in all three ice cores, between the two Öræfajökull deposits, that could act as a stratigraphic marker.

4.2. Key deposits missing from the ice core framework

Despite the high resolution and continuous sampling over broad intervals, key LGIT tephras such as the Laacher See Tephra (LST), Penifiler Tephra, Glacier Peak and Neapolitan Yellow Tuff of GI-1 and Y-1, Greenish and Pomici di Base of GS-2 (Fig. 2), have not been identified in Greenland. We did not find any deposits with trachyte, trachydacite or trachy-andesite compositions, that could be indicative of products from the Mediterranean, Azores, Jan Mayen, Massif Central or Eifel regions (Fig. 1). This 'regional absence' extends from the Holocene to the Eemian and raises questions as to the dominant barrier to dispersal of tephra in a north-western direction from central and southern Europe, despite numerous explosive eruptions (e.g Riede, 2008; Wulf et al., 2012). The absence of prominent Plinian events suggests that external mechanisms influence northern transport of tephra, and barriers could include wind patterns or the Polar Front Jet Stream. For example, the LST from Germany, of GI-1 age, is a key isochron that could help assess synchroneity of the GS-1 onset between Europe and the Arctic. The LST remains elusive in Greenland despite sampling three ice cores, over depth ranges that encompass best age estimates (Bronk Ramsey et al., 2015; Reinig et al., 2021; Abbott et al., 2021). In novel simulations, Niemeier et al. (2021) find that both radiative heating of ash as well as rotation influence distribution pathways, which most likely led to LST ash dispersal to the south and east.

Contrary to high Holocene eruption frequencies, the first continuous reconstruction of LGIT volcanism from Kamchatkan Peninsula deposits (Ponomareva et al., 2021) reveals lower volcanic activity with infrequent, less explosive events between 30 and 12 ka BP. This could explain why no Kamchatkan tephra horizons were identified in the Greenland LGIT tephra framework.

5. Conclusions

- This study significantly improves our knowledge of Icelandic volcanism during the LGIT and aids the validation and/or transfer of the GICC05 timescale between Greenland ice cores, particularly during GS-2.1a.
- The framework provides a focus for future studies seeking to assess the regional development of rapid climatic events across ice, marine and terrestrial records - a key aim of the INTIMATE project. We highlight at least 23 layers that hold most potential for these purposes (Fig. 8), including a Hekla-Vatnafjöll or

Fig. 13. Major element-element biplots showing the geochemical relationship between ice-core deposits and terrestrial and/or marine deposits (normalised to 100%), excluding totals <94 wt%. Error bars represent 2σ of replicate analyses of the BCR2g and Lipari obsidian secondary standards, for basalt and rhyolitic analyses respectively. (T) = terrestrial and (M) = marine deposits. (A–D) NEEM 1429.13 m against Vedde Ash deposits from MD99-2271 (M) (Guðmundsdóttir et al., 2011) and Loch Ashik (T) (Lane et al., 2012). (E–H) NGRIP 1557.60 m compared to Pyne-O'Donnell et al. (2016) data from Thin Ice Pond, Nova Scotia - MSH set JY (T) Veinot Lake, Nova Scotia – MSH set J (T), Crocker Pond, Maine USA - MSH set J (T) and proximal reference UA2482– JY (T). (M–P) and (I–L) NEEM 1472.35 m, NGRIP 1573.00 m and GRIP 1716.40 m with basaltic GI-1d layers from Lock Ashik Isl-W, Scotland (T) from Pyne-O'Donnell et al. (2008) and North Atlantic core RAPiD-15–4P (M) (Thornalley et al., 2011). (Q–T) NEEM 1502.60 m and NGRIP 1628.25 m against proximal Shingo Village samples (T) (Aoki and Machida, 2006) and deposits from the Forearc terrace of the Japan Trench, from ODP cores Hole 1150A, 1151C and KH94-3 LM-8 A, 1151C and KH94-3, LM-8 (M) (Aoki and Sakamoto, 2003).

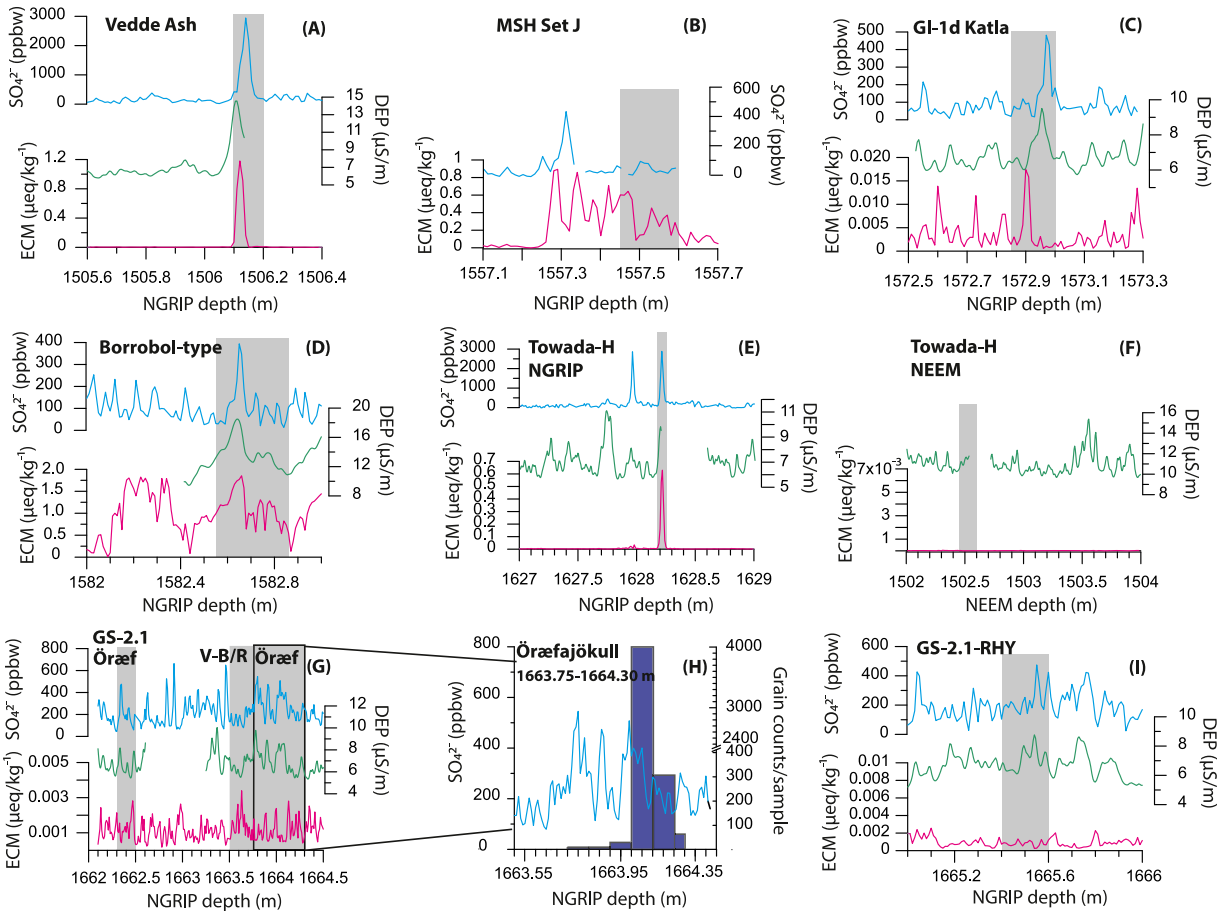

Fig. 14. (A–I): A selection of NGRIP tephra deposits and one NEEM deposit (F) shown together with ECM, DEP and SO_4^{2-} measurements over depth intervals within which tephra deposits were found. Tephra sampling was conducted over depth intervals denoted by grey shading. (H) shows the high-resolution grain counts of an Öræfajökull deposit against SO_4^{2-}.

Vestmannaeyjar deposit located at the Holocene transition, a MSH set J event, a GI-1d-Katla, and a series of GS-2.1a deposits

- The isochrons originating from Öræfajökull in GS-2.1a have not yet been identified proximally in Iceland, nor in other regional climate archives and creates opportunities to research Icelandic silicic volcanism and GS-2.1a tephrochronology.
- We recommend that ice-core tephra deposits are included in future regional and global eruption frequency estimates alongside chemostratigraphic markers. Seventy percent of NGRIP tephra deposits presented here occur with associated ECM, DEP or SO_4^{2-} peaks meaning calculations of LGIT volcanism, especially from smaller eruptions remain underestimated.
- The continuous direct ice sampling method is most reliable for locating the maximum number of tephra deposits in the ice and creating a comprehensive tephra record within a targeted interval.

Author contributions

Eliza Cook: Conceptualization, Methodology, Formal analysis, Investigation, Visualization, Validation, Writing - Original Draft, Writing - Review & Editing. **Siwan M. Davies:** Conceptualization, Methodology, Funding Acquisition, Resources, Writing - Review & Editing, Supervision. **Peter M. Abbott:** Methodology, Supervision, Writing - Review & Editing. **Nick J.G. Pearce:** Methodology, Resources, Writing - Review & Editing. **Seyedhamidreza Mojtabavi:** Formal analysis, Writing - Review & Editing **Anders Svensson:** Methodology, Writing - Review & Editing. **Anna J. Bourne:** Investigation, Writing - Review & Editing. **Inger K. Seierstad:** Investigation, Writing - Review & Editing. **Sune O. Rasmussen:** Writing - Review & Editing. **Bo M. Vinther:** Funding Acquisition. **Joseph Harrison:** Investigation. **Elliott Street:** Investigation. **Jørgen Peder Steffensen,** Methodology. **Frank Wilhelms:** Methodology.

Declaration of competing interest

The authors declare that they have no known competing financial interests or personal relationships that could have appeared to influence the work reported in this paper.

Acknowledgements

EC was supported by PhD studentship funding from Swansea University. EC, SMD, AJB and PMA were supported by the European Research Council (ERC) project Tephra constraints on Rapid Climate Events (TRACE project: 259253). Financial and laboratory funding was provided to EC from the ERC under the European Community's Seventh Framework Programme (FP7/2007–2013)/ERC grant agreement 610055 as part of the ice2ice project. This is also a TiPES contribution #129, having received funding from the European

Union's Horizon 2020 research and innovation programme under grant agreement no 820970. This research contributes to the NGRIP and NEEM ice-core projects, which are curated by Physics of Ice, Climate and Earth (PICE), Niels Bohr Institute, University of Copenhagen (KU). These projects were supported by funding agencies in Denmark (SNF, FI), Canada (NRCan/GSC), China (CAS), Belgium (FNRS-CFB, FWO), France (IPEV, IFRTP, INSU/CNRS, CEA and ANR), Germany (AWI), Iceland (RannIs), Japan (MEXT, NIPR), South Korea (KOPRI), Sweden (SPRS, VR), Switzerland (SNF), The Netherlands (NWO/ALW), United Kingdom (NERC) and the United States of America (NSF, Office of Polar Programs). EC was supported by STSM funding from EU-COST INTIMATE action (ES0907) to conduct ice sampling at KU, and by the Quaternary Research Association to conduct LA-ICP-MS analyses at Aberystwyth University. PA received funding from the European Research Council under the European Union's Horizon 2020 research and innovation programme (grant agreement no. 820047). We thank Dr Chris Hayward assistance at TAU, and Rhys Timms, Sean Pyne-O'Donnell and Britta Jensen for discussions on MSH geochemistry, and two anonymous reviewers for their valuable feedback.

Appendix A. Supplementary data

Supplementary data to this article can be found online at https://doi.org/10.1016/j.quascirev.2022.107596.

References

Abbott, P.M., Davies, S.M., Steffensen, J.P., Pearce, N.J.G., Bigler, M., Johnsen, S.J., Seierstad, I., Svensson, A., Wastegård, S., 2012. A detailed framework of marine isotope stages 4 and 5 volcanic events recorded in two Greenland ice-cores. Quat. Sci. Rev. 36, 59–77. https://doi.org/10.1016/j.quascirev.2011.05.001.

Abbott, P.M., Davies, S.M., 2012. Volcanism and the Greenland ice-cores: the tephra record. Earth Sci. Rev. 11, 173–191. https://doi.org/10.1016/j.earscirev.2012.09.001.

Abbott, P.M., Plunkett, G., Corona, C., Chellman, N.J., McConnell, J.R., Pilcher, J.R., Stoffel, M., Sigl, M., 2021. Identification of cryptotephra from the Icelandic Veiðivötn 1477 CE eruption in a Greenland ice core: role in confirming the dating of volcanic events in the 1450s CE and assessing the eruption's climatic impact. Clim. Past. 17 (2), 565–585. https://doi.org/10.5194/cp-17-565-2021.

Abbott, P.M., Niemeier, U., Timmreck, C., Riede, F., McConnell, J.R., Severi, M., Fischer, H., Svensson, A., Toohey, M., Reinig, F., Sigl, M., 2021. Volcanic climate forcing preceding the inception of the Younger Dryas: implications for tracing the Laacher See eruption. Quat. Sci. Rev. 274, 107260. https://doi.org/10.1016/j.quascirev.2021.107260.

Andersen, K.K., Svensson, A., Johnsen, S.J., Rasmussen, S.O., Bigler, M., Röthlisberger, R., Ruth, U., Siggaard-Andersen, M.-L., Steffensen, J.P., Dahl-Jensen, D., Vinther, B.M., Clausen, H.B., 2006. The Greenland Ice Core Chronology 2005, 15–42 ka. Part 1: constructing the time scale. Quat. Sci. Rev. 25, 3246–3257. https://doi.org/10.1016/j.quascirev.2006.08.002.

Aoki, K., Arai, F., 2000. Late quaternary tephrostratigraphy of marine core KH94-3, LM-8 off sanriku, Japan. Quater. Res. 39, 107–120.

Aoki, K., Machida, H., 2006. Major element composition of volcanic glass shards in the late Quaternary widespread tephras in Japan - distinction of tephras using K_2O-TiO_2 diagrams. Bull. Geol. Surv. Jpn. 57, 239–258.

Aoki, K., Sakamoto, T., 2003. Late quaternary tephrostratigraphy of the sediments from the Japan trench forearc, holes 1150A and 1151C. In: Suyehiro, K., Sacks, I.S., Acton, G.D., Oda, M. (Eds.), Proceedings of the Ocean Drilling Program, Scientific Results, vol. 186, pp. 1–22.

Bigler, M., 2004. Hochauflösende Spurenstoffmessungen an polaren Eisbohrkernen: Glazio-chemische und klimatische Prozessstudien. Ph.D. thesis. Physics Institute, University of Bern, Switzerland, 2004.

Bigler, M., Svensson, A., Steffensen, J.P., Kaufmann, P., 2007. A new continuous high-resolution detection system for sulphate in ice cores. Ann. Glaciol. 45 (1), 178–182. https://doi.org/10.3189/172756407782282471.

Björck, S., Walker, M.J.C., Cwynar, L., Johnsen, S.J., Knudsen, K.L., Lowe, J.J., Wohlfarth, B., INTIMATE Members, 1998. An event stratigraphy for the last termination in the North Atlantic region based on the Greenland Ice Core record: a proposal by the INTIMATE group. J. Quat. Sci. 13, 283–292. https://doi.org/10.1002/(SICI)1099-1417(199807/08)13:4<283::AID-JQS386>3.0.CO;2-A.

Blockley, S.P.E., Lane, C.S., Hardiman, M., Rasmussen, S.O., Seierstad, I.K., Steffensen, J.P., Svensson, A., Lotter, A.F., Turney, C.S.M., Bronk Ramsey, C., INTIMATE members, 2012. Synchronisation of palaeoenvironmental records over the last 60,000 years, and an extended INTIMATE event stratigraphy to 48,000 b2k. Quat. Sci. Rev. 36, 2–10. https://doi.org/10.1016/j.quascirev.2011.09.017.

Borchardt, G.A., Aruscavage, P.J., Millard, H.J., 1972. Correlation of the Bishop Ash, a Pleistocene marker bed, using instrumental neutron activation analysis. J. Sediment. Res. 42 (2), 301–306. https://doi.org/10.1306/74D72527-2B21-11D7-8648000102C1865D.

Bourne, A.J., Davies, S.M., Abbott, P.M., Rasmussen, S.O., Steffensen, J.P., Svensson, A., 2013. Revisiting the Faroe Marine Ash Zone III in two Greenland ice cores: implications for marine-ice correlations. J. Quat. Sci. 28, 641–646. https://doi.org/10.1002/jqs.2663.

Bourne, A.J., Cook, E., Abbott, P.M., Seierstad, I.K., Steffensen, J.P., Svensson, A., Fischer, H., Schupbach, S., Davies, S.M., 2015. A tepra lattice for Greenland and a reconstruction of volcanic events spanning 25-45 ka b2k. Quat. Sci. Rev. 118, 122–141. https://doi.org/10.1016/j.quascirev.2014.07.017.

Bourne, A.J., Abbott, P.M., Albert, P.G., Cook, E., Pearce, N.J.G., Ponomareva, V., Svensson, A., Davies, S.M., 2016. Underestimated risks of recurrent long-range ash dispersal from northern Pacific Arc volcanoes. Sci. Rep. 6, 29837. https://doi.org/10.1038/srep29837.

Bronk Ramsey, C., Albert, P.G., Blockley, S.P., Hardiman, M., Housley, R.A., Lane, C.S., Lee, S., Matthews, I.P., Smith, V.C., Lowe, J.J., 2015. Improved age estimates for key Late Quaternary European tephra horizons in the RESET lattice. Quat. Sci. Rev. 118, 18–32. https://doi.org/10.1016/j.quascirev.2014.11.007.

Calanchi, N., Dinelli, E., Lucchini, F., Mordenti, A., 1996. Chemostratigraphy of late quaternary sediments from lake albano and central adriatic sea cores (PALICLAS project). Mem. Ist. ital. Idrobiol. 55, 247–263.

Cook, E., Davies, S.M., Guðmundsdóttir, E.R., Abbott, P.M., Pearce, N.J.G., 2018a. First identification and characterization of Borrobol-type tephra in the Greenland ice cores: new deposits and improved age estimates. J. Quat. Sci. 33 (2), 212–224. https://doi.org/10.1002/jqs.3016.

Cook, E., Portnyagin, M., Ponomareva, V., Bazanova, L., Svensson, A., Garbe-Schönberg, D., 2018b. First identification of cryptotephra from the Kamchatka Peninsula in a Greenland ice core: implications of a widespread marker deposit that links Greenland to the Pacific northwest. Quat. Sci. Rev. 181, 200–206. https://doi.org/10.1016/j.quascirev.2017.11.036.

Clausen, H.B., Hammer, C.U., Hvidberg, C.S., Dahl-Jensen, D., Steffensen, J.P., Kipfstuhl, S., Legrand, M., 1997. A comparison of the volcanic records over the past 4000 years from the Greenland Ice Core Project and Dye 3 Greenland ice cores. J. Geophys. Res. 102 (C12), 26,707–726,723. https://doi.org/10.1029/97JC00587.

Clynne, M.A., Calvert, A.T., Wolfe, E.W., Evarts, R.C., Fleck, R.J., Lanphere, M.A., 2008. The Pleistocene eruptive history of Mount St. Helens, Washington, from 300,000 to12,800 years before present. In: Sherrod, D.R., Scott, W.E., Stauffer, P.H. (Eds.), A Volcano Rekindled: the Renewed Eruption of Mount St. Helens. https://doi.org/10.3133/pp175028, 2004-2006. 1750-28. 593–627, USGS Professional Paper.

Dansgaard, W., Johnsen, S.J., Clausen, H.B., Dahl-Jensen, D., Gundestrup, N.S., Hammer, C.U., Hvidberg, C.S., Steffensen, J.P., Sveinbjörnsdottir, A.E., Jouzel, J., Bond, G., 1993. Evidence for general instability of past climate from a 250-kyr ice-core record. Nature 364, 218–220. https://doi.org/10.1038/364218a0.

Davies, S.M., Branch, N.P., Lowe, J.J., Turney, C.S.M., 2002. Towards a European tephrochronological framework for termination 1 and the early Holocene. Philos. Trans. A Math Phys. Eng. Sci. 360 (1793), 767–802. https://doi.org/10.1098/rsta.2001.0964.

Davies, S.M., Wastegård, S., Rasmussen, T., Svensson, A., Johnsen, S.J., Steffensen, J.P., Andersen, K.K., 2008. Identification of the Fugloyarbanki tephra in the NGRIP ice core: a key tie-point for marine and ice-core sequences during the last glacial period. J. Quat. Sci. 23, 409–414. https://doi.org/10.1002/jqs.1182.

Davies, S.M., Wastegård, S., Abbott, P.M., Barbante, C., Bigler, M., Johnsen, S.J., Rasmussen, T.L., Steffensen, J.P., Svensson, A., 2010. Tracing volcanic events in the NGRIP ice-core and synchronising North Atlantic marine records during the Last Glacial period. Earth Planet Sci. Lett. 294 (1–2), 69–79. https://doi.org/10.1016/j.epsl.2010.03.004.

Davies, S., Abbott, P., Meara, R., Pearce, N., Austin, W., Chapman, M., Svensson, A., Bigler, M., Rasmussen, T., Rasmussen, S., Farmer, E., 2014. A North Atlantic tephrostratigraphical framework for 130–60 ka b2k: new tephra discoveries, marine-based correlations, and future challenges. Quat. Sci. Rev. 106, 101–121. https://doi.org/10.1016/j.quascirev.2014.03.024.

Davies, S.M., 2015. Cryptotephras: the revolution in correlation and precision dating. J. Quat. Sci. 30, 114–130. https://doi.org/10.1002/jqs.2766.

Deino, A.L., Orsi, G., de Vita, S., Piochi, M., 2004. The age of the neapolitan yellow Tuff caldera-forming eruption (Campi Flegrei caldera Italy) assessed by 40Ar/39Ar dating method. J. Volcanol. Geoth. Res. 133 (1–4), 157–170. https://doi.org/10.1016/S0377-0273(03)00396-2.

Denton, J.S., Pearce, N.J.G., 2008. Comment on Vinther et al. "A synchronized dating of three Greenland ice cores throughout the Holocene": the Minoan tephra is not present in the 1642 B.C. layer of the GRIP ice core. J. Geophys. Res. 113, D04303. https://doi.org/10.1029/2007JD008970.

Dunbar, N.W., Kurbatov, A.V., 2011. Tephrochronology of the Siple Dome ice core, West Antarctica: correlations and sources. Quat. Sci. Rev. 30 (13–14), 1602–1614. https://doi.org/10.1016/j.quascirev.2011.03.015.

Fisher, R.V., 1961. Proposed classification of volcanoclastic sediments and rocks. Geol. Soc. Am. Bull. 72 (9), 1409–1414. https://doi.org/10.1130/0016-7606(1961)72[1409:PCOVSA]2.0.CO, 2.

Fuhrer, K., Neftel, A., Anklin, M., Staffelbach, T., Legrand, M., 1996. High-resolution ammonium ice core record covering a complete glacial-interglacial cycle. J. Geophys. Res. 101 (D2), 4147–4164. https://doi.org/10.1029/95JD02903.

Gautier, E., Savarino, J., Hoek, J., Erbland, J., Caillon, N., Hattori, S., Yoshida, N., Albalat, E., Albarede, F., Farquhar, F., 2019. 2600-years of stratospheric volcanism through sulfate isotopes. Nat. Commun. 10, 466. https://doi.org/10.1038/s41467-019-08357-0.

Gkinis, V., Vinther, B.M., Popp, T.J., Quistgaard, T., Faber, A., Holme, C.T., Jensen, C., Lanzky, M., Luett, A., Mandrakis, V., Orum, N., Pedersen, A., Vaxevani, N., Weng, Y., Capron, E., Dahl-Jensen, D., Hoerhold, M., Jones, T.R., Jouzel, J., Landais, A., Masson-Delmotte, V., Oerter, H., Rasmussen, Sune Olander, Steen-Larsen, H.C., Steffensen, J.P., Sveinbjörnsdóttir, A., Svensson, A., Vaughn, B., White, J.W.C., 2021. A 120,000-year long climate record from a NW-Greenland deep ice core at ultra-high resolution. Sci. Data 8, 141. https://doi.org/10.1038/s41597-021-00916-9.

Grönvold, K., Óskarsson, N., Johnsen, S.J., Clausen, H.B., Hammer, C.U., Bond, G., Bard, E., 1995. Ash layers from Iceland in the Greenland GRIP ice core correlated with oceanic and land sediments. Earth Planet Sci. Lett. 135 (1–4), 149–155. https://doi.org/10.1016/0012-821X(95)00145-3.

Guðmundsdóttir, E., Eiríksson, J., Larsen, G., 2011. Identification and definition of primary and reworked tephra in Late Glacial and Holocene marine shelf sediments off North Iceland. J. Quat. Sci. 26 (6), 589–602. https://doi.org/10.1002/jqs.1474.

Hammer, C.U., 1980. Acidity of polar ice cores in relation to absolute dating, past volcanism, and radio-echoes. J. Glaciol. 25 (93), 359–372. https://doi.org/10.3189/S0022143000015227.

Hayakawa, Y., 1985. Pyroclastic Geology of Towada Volcano, vol. 60. Bulletin of the Earthquake Research Institute, Uni. Tokyo, pp. 507–592.

Hayward, C., 2012. High spatial resolution electron probe microanalysis of tephras and melt inclusions without beam-induced chemical modification. Holocene 22, 119–125.

Hunt, J., Hill, P.G., 1993. Tephra geochemistry: a discussion of some persistent analytical problems. Holocene 3 (3), 271–278. https://doi.org/10.1177/095968369300300310.

Hunt, J.B., Fannin, G.T., Hill, P.G., Peacock, J.D., 1995. The Tephrochronology and Radiocarbon Dating of North Atlantic, Late-Quaternary Sediments: an Example from the St. Kilda Basin, vol. 90. Geological Society, London, Special Publications, pp. 227–240. https://doi.org/10.1144/GSL.SP.1995.090.01.15.

Ikehara, K., Ohkushi, K., Noda, A., Danhara, T., Yamashita, T., 2013. A new local marine reservoir correction for the last deglacial period in the Sanriku region, northwestern North Pacific, based on radiocarbon dates from the Towada-Hachinohe (To-H) tephra. Quater. Res. 52 (4), 127–137. https://doi.org/10.4116/jaqua.52.127.

Irvine, T.N., Baragar, W.R.A., 1971. A guide to the chemical classification of the common volcanic rocks. Can. J. Earth Sci. 8, 523–548. https://doi.org/10.1139/e71-055.

Jarvis, R.J.V., 2013. Palaeoceanographic and Climatic Changes during the Late Weichselian and the Holocene off North Iceland: Foraminifera and Stable Isotopes. MSc Thesis. University of Aarhus.

Jensen, B.J.L., Pyne-O'Donnell, S., Plunkett, G., Froese, D.G., Hughes, P.D.M., Sigl, M., McConnell, J.R., Amesbury, M.J., Blackwell, P.G., van den Bogaard, C., Buck, C.E., Charman, D.J., Clague, J.J., Hall, V.A., Koch, J., Mackay, H., Mallon, G., McColl, L., Pilcher, J.R., 2014. Transatlantic distribution of the alaskan white river ash. Geology 42 (10), 875–878. https://doi.org/10.1130/G35945.1.

Johnsen, S.J., Clausen, H.B., Dansgaard, W., Fuhrer, K., Gundestrup, N., Hammer, C.U., Iversen, P., Steffensen, J.P., Jouzel, J., Stauffer, B., 1992. Irregular glacial interstadials recorded in a new Greenland ice core. Nature 359, 311–313. https://doi.org/10.1038/359311a0.

Johnsen, S.J., Dahl-Jensen, D., Gundestrup, N., Steffensen, J.P., Clausen, H.B., Miller, H., Masson-Delmotte, V., Sveinbjörnsdóttir, A.E., White, J., 2001. Oxygen isotope and palaeotemperature records from six Greenland ice-core stations: camp Century, Dye-3, GRIP, GISP2, Renland and NorthGRIP. J. Quat. Sci. 16, 299–307. https://doi.org/10.1016/1040-6182(95)00075-5.

Juvigné, E.H., Bastin, B., Delibrias, G., Evin, J., Gewelt, M., Gilot, E., Streel, M., 1996. A comprehensive pollen- and tephra-based chronostratigraphic model for the Late Glacial and Holocene period in the French Massif Central. Quat. Int. 34–36, 113–120.

Kaufmann, P.R., Federer, U., Hutterli, M.A., Bigler, M., Schupbach, S., Ruth, U., Schmitt, J., Stocker, T., 2008. An improved continuous flow analysis system for high-resolution field measurements on ice cores. Environ. Sci. Technol. 42 (21), 8044–8050. https://doi.org/10.1021/es8007722.

Koren, J.H., Svenden, J.I., Mangerud, J., Furnes, H., 2008. The Dimna Ash - a 12.8 14C ka-old volcanic ash in Western Norway. Quat. Sci. Rev. 27 (1–2), 85–94. https://doi.org/10.1016/j.quascirev.2007.04.021.

Kuehn, S., Froese, D., Carrara, P., Foit, F., Pearce, N., Rotheisler, P., 2009. Major- and trace-element characterization, expanded distribution, and a new chronology for the latest Pleistocene Glacier Peak tephras in western North America. Quat. Res. 71 (2), 201–216. https://doi.org/10.1016/j.yqres.2008.11.003.

Kurbatov, A.V., Zielinski, G.A., Dunbar, N.W., Mayewski, P.A., Meyerson, E.A., Sneed, S.B., Taylor, K.C., 2006. A 12,000 year record of explosive volcanism in the siple dome ice core, west Antarctica. J. Geophys. Res. 111, D12307. https://doi.org/10.1029/2005JD006072.

Lane, C.S., Blockley, S.P.E., Mangerud, J., Smith, V.C., Lohne, Ø.S., Tomlinson, E.L., Matthews, I.P., Lotter, A.F., 2012. Was the 12.1 ka Icelandic Vedde Ash one of a kind? Quat. Sci. Rev. 33, 87–99. https://doi.org/10.1016/j.quascirev.2011.11.011.

Lane, C.S., Brauer, A., Blockley, S.P.E., Dulskim, P., 2013. Volcanic ash reveals time-transgressive climate change during the Younger Dryas. Geology 41 (12), 1251–1254. https://doi.org/10.1130/G34867.1.

Le Maitre, R.W., Streckeisen, A., Zanettin, B., Le Bas, M.J., Bonin, B., Bateman, P., Bellieni, G., Dudek, A., Efremova, S., Keller, J., Lameyre, J., 2002. Igneous Rocks. A Classification and Glossary of Terms: Recommendations of the International Union of Geological Sciences Subcommission on the Systematics of Igneous Rocks, second ed. Cambridge University Press, Cambridge, p. 236.

Lin, J., Svensson, A., Hvidberg, C.S., Lohmann, J., Kristiansen, S., Dahl-Jensen, D., Steffensen, J.P., Rasmussen, S.O., Cook, E., Kjær, H.A., Vinther, B.M., Fischer, H., Stocker, T., Sigl, M., Bigler, M., Severi, M., Traversi, R., Mulvaney, R., 2022. Magnitude, frequency and climate forcing of global volcanism during the last glacial period as seen in Greenland and Antarctic ice cores (60–9 ka). Clim. Past. 18, 485–506. https://doi.org/10.5194/cp-18-485-2022.

Lind, E.M., Lilja, C., Wastegård, S., Pearce, N.J.G., 2016. Revisiting the Borrobol tephra. Boreas 45 (4), 629–643. https://doi.org/10.1111/bor.12176.

Lowe, D.J., Hunt, J.B., 2001. A summary of terminology used in tephra related studies. In: Juvigne, E.R., P (Eds.), Tephras, Chronology and Archaeology: Les Dossiers de l'Archaeo-logis 1. Goudet: France, pp. 17–22.

Lowe, D.J., 2011. Tephrochronology and its application: a review. Quat. Geology. 6 (2), 107–153. https://doi.org/10.1016/j.quageo.2010.08.003.

Lowe, D.J., Pearce, N.J.G., Jorgensen, M.A., Kuehn, S.C., Tryon, C.A., Hayward, C.L., 2017. Correlating tephras and cryptotephras using glass compositional analyses and numerical and statistical methods: review and evaluation. Quat. Sci. Rev. 175, 1–44. https://doi.org/10.1016/j.quascirev.2017.08.003.

Lowe, J.J., Rasmussen, S.O., Björck, S., Hoek, W.Z., Steffensen, J.P., Walker, M.J.C., Z, C., 2008. Synchronisation of palaeoenvironmental events in the North Atlantic region during the Last Termination: a revised protocol recommended by the INTIMATE group. Quat. Sci. Rev. 27 (1–2), 6–17. https://doi.org/10.1016/j.quascirev.2007.09.016.

Machida, H., Arai, F., 2003. In: Atlas of Tephra in and Around Japan (Rev. University of Tokyo Press, Tokyo.

Mangerud, J., Lie, S.E., Furnes, H., Kristiansen, I.L., Lømo, L., 1984. A younger Dryas ash bed in western Norway, and its possible correlations with tephra in cores from the Norwegian sea and the north atlantic. Quat.y Res. 21, 85–104. https://doi.org/10.1016/0033-5894(84)90092-9.

Matthews, I.P., Birks, H.A., Bourne, A.J., Brooks, S.J., Lowe, J.J., Macleod, A., Pyne-O'Donnell, S.D.F., 2011. New age estimates and climatostratigraphic correlations for the Borrobol and penifiler tephras: evidence from Abernethy forest, Scotland. J. Quat. Sci. 26, 247–252. https://doi.org/10.1002/jqs.1498.

McDonough, W.F., Sun, S.S., 1995. The composition of the earth. Chem. Geol. 120 (3–4), 223–253. https://doi.org/10.1016/0009-2541(94)00140-4.

Mojtabavi, S., Eisen, O., Franke, S., Jansen, D., Steinhage, D., Dahl-Jensen, D., Paden, J., Weikusat, I., Eichler, J., Wilhelms, F., 2022. Origin of englacial stratigraphy at three deep ice core sites of the Greenland Ice Sheet by synthetic radar modelling. J. Glaciology. 1–13. https://doi.org/10.1017/jog.2021.137.

Mojtabavi, S., Wilhelms, F., Cook, E., Davies, S.M., Sinnl, G., Skov Jensen, M., Dahl-Jensen, D., Svensson, A., Vinther, B.M., Kipfstuhl, S., Jones, G., Karlsson, N.B., Faria, S.H., Gkinis, V., Kjær, H.A., Erhardt, T., Berben, S.M.P., Nisancioglu, K.H., Koldtoft, I., Rasmussen, S.O., 2020. A first chronology for the East Greenland Ice-core Project (EGRIP) over the Holocene and last glacial termination. Clim. Past 16, 2359–2380. https://doi.org/10.5194/cp-16-2359-2020.

Moore, J.C., Wolff, E.W., Clausen, H.B., Hammer, C.U., 1992. The chemical basis for the electrical stratigraphy of ice. J. Geophys. Res. 97, 1887–1896. https://doi.org/10.1029/91JB02750.

Mortensen, A.K., Bigler, M., Grönvold, K., Steffensen, J.P., Johnsen, S.J., 2005. Volcanic ash layers from the Last Glacial Termination in the NGRIP ice core. J. Quat. Sci. 20, 209–219. https://doi.org/10.1002/jqs.908.

Mullineaux, D.R., 1996. Pre-1980 Tephra-fall Deposits Erupted from Mount St. Helens. USGS Professional Paper 1563. United States Government Printing Office, Washington, p. 109.

Narcisi, B., 1996. Tephrochronology of a Late Quaternary lacustrine record from the Monticchio maar (Vulture volcano, southern Italy). Quat. Sci. Rev. 15, 155–165. https://doi.org/10.1016/0277-3791(95)00045-3.

Niemeier, U., Riede, F., Timmreck, C., 2021. Simulation of ash clouds after a Laacher See-type eruption. Clim. Past. 17, 633–652. https://doi.org/10.5194/cp-17-633-2021.

NGRIP members, 2004. High-resolution record of Northern Hemisphere climate extending into the last interglacial period. Nature 431, 147–151. https://doi.org/10.1038/nature02805.

Ogawa, A., Kurita, H., Ganzawa, Y., 2011. SAR-RTL and IRTL dating of volcanic single quartz grain extracted from Towada-Hachinohe (To-H) pyroclastic flow. Quat. Res. 50, 169–180. https://doi.org/10.4116/jaqua.50.169 (J+E).

Pearce, N.J.G., Perkins, W.T., Westgate, J.A., Gorton, M.P., Jackson, S.E., Neal, C.R., Chenery, S.P., 1997. A compilation of new and published major and trace element data for NIST SRM 610 and NIST SRM 612 glass reference materials. Geostand. Newsl. 21, 115–144. https://doi.org/10.1111/j.1751-908X.1997.tb00538.x.

Pearce, N.J.G., Westgate, J.A., Eastwood, W.J., Preece, S.J., Perkins, W.T., 2004a. Identification of Aniakchak (Alaska) tephra in Greenland ice core challenges the 1645BC date for the Minoan eruption of Santorini. G-cubed 5, Q03005. https://doi.org/10.1029/2003GC000672.

Pearce, N.J.G., Westgate, J.A., Perkins, W.T., Preece, S.J., 2004b. The application of ICP-MS methods to tephrochronological problems. Appl. Geochem. 19, 289–322. https://doi.org/10.1016/S0883-2927(03)00153-7.

Pearce, N.J.G., Alloway, B.V., Westgate, J.A., 2008. Mid-Pleistocene silicic tephra beds in the Auckland region, New Zealand: their correlation and origins based on the trace element analyses of single glass shards. Quat. Int. 178 (1), 16–43. https://

doi.org/10.1016/j.quaint.2006.09.005.
Pearce, N.J.G., Perkins, W.T., Westgate, J.A., Wade, S.C., 2011. Trace element analysis by laser ablation ICP-MS: the quest for comprehensive chemical characterisation of single sub-10um volcanic glass shards. Quat. Int. 246 (1–2), 57–81. https://doi.org/10.1016/j.quaint.2011.07.012.
Pearce, N.J.G., Abbott, P.M., Martin-Jones, C., 2014. Microbeam methods for the analysis of glass in fine-grained tephra deposits: a SMART perspective on current and future trends. In: Austin, W.E.N., Abbott, P.M., Davies, S.M., Pearce, N.J.G., Wastegård, S. (Eds.), Marine Tephrochronology, vol. 398. Geological Society, London, Special Publications, pp. 29–45.
Perkins, M.E., Nash, W.P., Brown, F.H., Fleck, R.J., 1995. Fallout tuffs of trapper Creek, Idaho – a record of miocene explosive volcanism in the snake river plain volcanic province. *Bull.* Geol. Soc. Am. Bull. 107 (12), 1484–1506. https://doi.org/10.1130/0016-7606(1995)107<1484:FTOTCI>2.3.CO;2.
Perkins, M.E., Brown, F.H., Nash, W.P., McIntosh, W., Williams, S.K., 1998. Sequence, age, and source of silicic fallout tuffs in middle to late Miocene basins of the northern Basin and Range province. Geol. Soc. Am. Bull. 110 (3), 344–360. https://doi.org/10.1130/0016-7606(1998)110<0344:SAASOS>2.3.CO;2.
Ponomareva, V., Pendea, F., Zelenin, E., Portnyagin, M., Gorbach, N., Pevzner, M., Plechova, A., Derkachev, A., Rogozin, A., Garbe-Schönberg, D., 2021. The first continuous late Pleistocene tephra record from Kamchatka Peninsula (NW Pacific) and its volcanological and paleogeographic implications. Quat. Sci. Rev. 257, 106838. https://doi.org/10.1016/j.quascirev.2021.106838.
Pyne-O'Donnell, S.D.F., Blockley, S.P.E., Turney, C.S.M., Lowe, J.J., 2008. Distal volcanic ash layers in the Lateglacial Interstadial (GI-1): problems of stratigraphic discrimination. Quat. Sci. Rev. 27, 72–84. https://doi.org/10.1016/j.quascirev.2007.02.019.
Pyne-O'Donnell, S.D., Cwynar, L.C., Jensen, B.J., Vincent, J.H., Kuehn, S.C., Spear, R., Froese, D.G., 2016. West Coast volcanic ashes provide a new continental-scale Lateglacial isochron. Quat. Sci. Rev. 142, 16–25. https://doi.org/10.1016/j.quascirev.2016.04.014.
Rasmussen, S.O., Andersen, K.K., Svensson, A.M., Steffensen, J.P., Vinther, B.M., Clausen, H.B., Siggaard-Andersen, M.-L., Johnsen, S.J., Larsen, L.B., Dahl-Jensen, D., Bigler, M., Röthlisberger, R., Fischer, H., Goto-Azuma, K., Hansson, M.E., Ruth, U., 2006. A new Greenland ice core chronology for the last glacial termination. J. Geophys. Res. 111, D06102. https://doi.org/10.1029/2005JD006079.
Rasmussen, S.O., Seierstad, I.K., Andersen, K.K., Bigler, M., Dahl-Jensen, D., Johnsen, S.J., 2008. Synchronization of the NGRIP, GRIP, and GISP2 ice cores across MIS 2 and palaeoclimatic implications. Quat. Sci. Rev. 27 (1–2), 18–28. https://doi.org/10.1016/j.quascirev.2007.01.016.
Rasmussen, S.O., Abbott, P.M., Blunier, T., Bourne, A.J., Brook, E., Buchardt, S.L., Buizert, C., Chappellaz, J., Clausen, H.B., Cook, E., Dahl-Jensen, D., Davies, S.M., Guillevic, M., Kipfstuhl, S., Laepple, T., Seierstad, I.K., Severinghaus, J.P., Steffensen, J.P., Stowasser, C., Svensson, A., Vallelonga, P., Vinther, B.M., Wilhelms, F., Winstrup, M., 2013. A first chronology for the North Greenland Eemian Ice Drilling (NEEM) ice core. Clim. Past 9, 2713–2730.
Rasmussen, S.O., Bigler, M., Blockley, S.P., Blunier, T., Buchardt, S.L., Clausen, H.B., Cvijanovic, I., Dahl-Jensen, D., Johnsen, S.J., Fischer, H., Gkinis, V., Guillevic, M., Hoek, W.Z., Lowe, J.J., Pedro, J.B., Popp, T., Seierstad, I.K., Steffensen, J.P., Svensson, A.M., Vallelonga, P., Vinther, B.M., Walker, M.J.C., Wheatley, J.J., Winstrup, M., 2014. A stratigraphic framework for abrupt climatic changes during the Last Glacial period based on three synchronized Greenland ice-core records: refining and extending the INTIMATE event stratigraphy. Quat. Sci. Rev. 106, 14–28. https://doi.org/10.1016/j.quascirev.2014.09.007.
Reinig, F., Wacker, L., Jöris, O., Oppenheimer, C., Guidobaldi, G., Nievergelt, D., Adolphi, F., Cherubini, P., Engels, S., Esper, J., Land, A., Lane, C., Pfanz, H., Remmele, S., Sigl, M., Sookdeo, A., Büntgen, U., 2021. Precise date for the laacher see eruption synchronizes the younger Dryas. Nature 595, 66–69. https://doi.org/10.1038/s41586-021-03608-x.
Riede, F., 2008. The laacher see-eruption (12,920 BP) and material culture change at the end of the allerød in northern Europe. J. Archaeol. Sci. 35 (3), 591–599. https://doi.org/10.1016/j.jas.2007.05.007.
Ruth, U., Wagenbach, D., Steffensen, J.P., Bigler, M., 2003. Continuous record of microparticle concentration and size distribution in the central Greenland NGRIP ice core during the last glacial period. J. Geophys. Res. 108 (D3), 4098. https://doi.org/10.1029/2002JD002376.
Sarna-Wojcicki, A.M., Meyer, C.E., Woodward, M.J., Lamothe, P.J., 1981. Composition of air-fall ash erupted on may 18, may 25, june 12, july 22 and august 7. In: Lipman, P.W., Mullineaux, D.R. (Eds.), The 1980 Eruptions of Mount St. Helens. Washington. United States Geological Survey Professional Paper 1250.
Seierstad, I.K., Abbott, P.M., Bigler, M., Blunier, T., Bourne, A.J., Brook, E., Buchardt, S.L., Buizert, C., Clausen, H.B., Cook, E., Dahl-Jensen, D., Davies, S.M., Guillevic, M., Johnsen, S.J., Pedersen, D.S., Popp, T.J., Rasmussen, S.O., Severinghaus, J., Svensson, A., Vinther, B.M., 2014. Consistently dated records from the Greenland GRIP, GISP2 and NGRIP ice cores for the past 104 ka reveal regional millennial-scale δ18O isotope gradients with possible Heinrich Event imprint. Quat. Sci. Rev. 106, 29–46. https://doi.org/10.1016/j.quascirev.2014.10.032.
Sinnl, G., Winstrup, M., Erhardt, T., Cook, E., Jensen, C.M., Svensson, A., Vinther, B.M., Muscheler, R., Rasmussen, S.O., 2022. A multi-ice-core, annual-layer-counted Greenland ice-core chronology for the last 3800 years: GICC21. Clim. Past. 18, 1125–1150. https://doi.org/10.5194/cp-18-1125-2022.
Smith, V.C., Isaia, R., Pearce, N.J.G., 2011. Tephrostratigraphy and glass compositions of post-15 kyr Campi Flegrei eruptions: implications for eruption history and chronostratigraphic markers. Quat. Sci. Rev. 30, 3638–3660. https://doi.org/10.1016/j.quascirev.2011.07.012.
Sigl, M., Winstrup, M., McConnell, J.R., Welten, K.C., Plunkett, G., Ludlow, F., Büntgen, U., Caffee, M., Chellman, N., Dahl-Jensen, D., Fischer, H., Kipfstuhl, S., Kostick, C., Maselli, O.J., Mekhaldi, F., Mulvaney, R., Muscheler, R., Pasteris, D.R., Pilcher, J.R., Salzer, M., Schüpbach, S., Steffensen, J.P., Vinther, B.M., Woodruff, T.E., 2015. Timing and climate forcing of volcanic eruptions for the past 2,500 years. Nature 523, 543–549. https://doi.org/10.1038/nature14565.
Sun, C., Plunkett, G., Liu, J., Zhao, H., Sigl, M., McConnell, J.R., Pilcher, J.R., Vinther, B., Steffensen, J.P., Hall, V., 2014. Ash from Changbaishan Millennium eruption recorded in Greenland ice: implications for determining the eruption's timing and impact. Geophys. Res. Lett. 41, 694–701. https://doi.org/10.1002/2013GL058642.
Svensson, A., Andersen, K.K., Bigler, M., Clausen, H.B., Dahl-Jensen, D., Davies, S.M., Johnsen, S.J., Muscheler, R., Rasmussen, S.O., Röthlisberger, R., Steffensen, J.P., Vinther, B.M., 2006. The Greenland Ice Core Chronology 2005, 15–42 ka. Part 2: comparison to other records. Quat. Sci. Rev. 25, 3258–3267. https://doi.org/10.1016/j.quascirev.2006.08.003.
Thórarinsson, S., 1944. Tefrokronologiska studier på Island. Geogr. Ann. 26, 1–217.
Thórarinsson, S., 1981. The applications of tephrochronology in Iceland. In: Self, S., Sparks, R.S.J. (Eds.), Tephra Studies (Proceedings of the NATO Advanced Study Institute 'Tephra Studies as a Tool in Quaternary Research'. D. Reidel, Dordrecht, pp. 109–134.
Thornalley, D.J.R., McCave, I.N., Elderfield, H., 2010. Freshwater input and abrupt deglacial climate change in the North Atlantic. Paleoceanography 25, PA1201. https://doi.org/10.1029/2009PA001772.
Thornalley, D.J.R., McCave, I.N., Elderfield, H., 2011. Tephra in deglacial ocean sediments south of Iceland: stratigraphy, geochemistry and oceanic reservoir ages. J. Quat. Sci. 26, 190–198. https://doi.org/10.1002/jqs.1442.
Timms, R., Matthews, I., Lowe, J., Palmer, A., Weston, D., Macleod, A., Blockley, S., 2019. Establishing tephrostratigraphic frameworks to aid the study of abrupt climatic and glacial transitions: a case study of the Last Glacial-Interglacial Transition in the British Isles (c. 16-8 ka BP). Earth Sci. Rev. 192, 34–64. https://doi.org/10.1016/j.earscirev.2019.01.003.
Turney, C.S.M., Harkness, D.D., Lowe, J.J., 1997. The use of microtephra horizons to correlate Late-glacial lake sediment successions in Scotland. J. Quat. Sci. 12, 525–531. https://doi.org/10.1002/(SICI)1099-1417(199711/12)12:6<525::AID-JQS347>3.0.CO;2-M.
van der Bilt, W.G., Lane, C.S., Bakke, J., 2017. Ultra-distal Kamchatkan ash on Arctic Svalbard: towards hemispheric cryptotephra correlation. Quat. Sci. Rev. 164, 230–235. https://doi.org/10.1016/j.quascirev.2017.04.007.
Vinther, B.M., Clausen, H.B., Johnsen, S.J., Rasmussen, S.O., Andersen, K.K., Buchardt, S.L., Dahl-Jensen, D., Seierstad, I.K., Siggaard-Andersen, M.-L., Steffensen, J.P., Svensson, A., Olsen, J., Heinemeier, J., 2006. A synchronised dating of three Greenland ice cores throughout the Holocene. J. Geophys. Res. 111, D13102. https://doi.org/10.1029/2005JD006921.
Wastegård, S., Gudmundsdóttir, E.R., Lind, E.M., Timms, R.G.O., Björck, S., Hannon, G.E., Olsen, J., Rundgren, M., 2018. Towards a Holocene tephrochronology for the Faroe Islands, North Atlantic. Quat. Sci. Rev. 195, 195–214. https://doi.org/10.1016/j.quascirev.2018.07.024.
Wilhelms, F., Kipfstuhl, J., Miller, H., Heinloth, K., Firestone, J., 1998. Precise dielectric profiling of ice cores: a new devise with improved guarding and its theory. J. Glaciol. 44 (146), 171–174. https://doi.org/10.3189/S002214300000246X.
Wilhelms, F., 2000. Messung dielektrischer Eigenschaften polarer. Berichte zur Polarforschung, Bremerhaven, Alfred Wegener Institute for Polar and Marine Research 367, 1–171.
Wolff, E.W., Moore, J.C., Clausen, H.B., Hammer, C.U., Kipfstuhl, S., Fuhrer, K., 1995. Long term changes in the acid and salt concentrations of the Greenland Ice Core Project ice cores from electrical stratigraphy. J. Geophys. Res. 100, 16,249–216,263. https://doi.org/10.1029/95JD01174.
Wolff, E., Moore, J., Clausen, H., Hammer, C., 1997. Climatic implications of background acidity and other chemistry derived from electrical studies of the Greenland Ice Core Project ice core. J. Geophys. Res. 102, 26325–26332. https://doi.org/10.1029/96JC02223.
Wolff, E.W., Cook, E., Barnes, P.R.F., Mulvaney, R., 2005. Signal variability in replicate ice cores. J. Glaciol. 51 (174), 462–468. https://doi.org/10.3189/172756505781829197.
Wulf, S., Keller, J., Paterne, M., Mingram, J., Lauterbach, S., Opitz, S., Sottili, G., Giaccio, B., Albert, P.G., Satow, C., Tomlinson, E.L., Viccaro, M., Brauer, A., 2012. The 100–133 ka record of Italian explosive volcanism and revised tephrochronology of Lago Grande di Monticchio. Quat. Sci. Rev. 58, 104–123. https://doi.org/10.1016/j.quascirev.2012.10.020.
Zielinski, G., Mayewski, P., Meeker, L., Whitlow, S., Twickler, M., 1996. A 110,000-yr record of explosive volcanism from the GISP2 (Greenland) ice core. Quat. Res. 45 (2), 109–118. https://doi.org/10.1006/qres.1996.0013.
Zolitschka, B., Negendank, J.F.W., Lottermoser, B.G., 1995. Sedimentological proof and dating of the early Holocene volcanic eruption of ulmener maar. Geol. Rundsch. 84, 213–219. https://doi.org/10.1007/BF00192252.